Work Order No. 582-22-31146-026
Contract No. 582-19-90500
Tracking No. 2022-25
Task 5.2

Prepared for:

Texas Commission on Environmental Quality
12100 Park 35 Circle MC 164
Austin, TX 78753

Prepared by:

Ramboll US Consulting, Inc.
7250 Redwood Blvd., Suite 105
Novato, California 94945

June 24, 2022

# Develop Tools to Process and Evaluate Options for Improved Fire Emission Inventories (EIs)

## Final Report

PREPARED UNDER A CONTRACT FROM THE
TEXAS COMMISSION ON ENVIRONMENTAL QUALITY

*The preparation of this document was financed through a contract from the State of Texas through the Texas Commission on Environmental Quality.*
*The content, findings, opinions and conclusions are the work of the author(s) and do not necessarily represent findings, opinions or conclusions of the TCEQ.*

RAMBOLL

# Develop Tools to Process and Evaluate Options for Improved Fire Emission Inventories (EIs)

## Final Report

Ramboll
7250 Redwood Boulevard
Suite 105
Novato, CA 94945
USA

T +1 415 899 0700
https://ramboll.com

# Contents



## Appendix

## Table of Figures

## Table of Tables

# EXECUTIVE SUMMARY

Fires are large emission sources and accurate Fire Emission Inventories (FEIs) are needed for exceptional event analyses and State Implementation Plan (SIP) modeling for ozone and regional haze. Currently available FEIs can differ by an order of magnitude (Li et al., 2020), so a well-developed FEI processing tool is essential to help understand the ranges of air quality impacts predicted using alternative FEIs in models such as the Comprehensive Air quality Model with extensions (CAMx). FEI processing is complex because the available inventories contain different information and omit some information needed by air quality models (e.g., daily temporal allocation, chemical speciation, and plume height profiles) requiring the use of supplementary data and assumptions. The TCEQ uses the Fire INventory from NCAR (FINN; Wiedinmyer et al., 2011) to estimate fire emissions, along with the Emissions Processing Software version 3 (EPS3) to prepare the FEI input into CAMx.

Ramboll developed a new literature-based Python FEI processor that provides the TCEQ a flexible fire emissions processing platform that can process four different FEIs which are 1) FINN1.0; 2) FINN2.5; 3) GFAS1.2, and 4) QFED2.5. The design of the FEI processor allows efficient future customization.

Comparisons of the three FEIs (we chose to evaluate FINN2.5 over FINN1.0 because it is the latest version available and is more similar to the FINN2.2 product that TCEQ is familiar with) revealed substantial differences in emissions of key pollutants for the 2019 ozone season in Texas as well as states that frequently contribute wildfire smoke into Texas. This finding is consistent with the literature review and highlights the uncertainties in fire detection and emissions estimations derived from satellite measurements. Testing and evaluation in CAMx can help to refine the emissions estimates produced by the FEI processor.

# 1.0 INTRODUCTION

## 1.1 Background

Fires are large emission sources and accurate Fire Emission Inventories (FEIs) are needed for exceptional event analyses and State Implementation Plan (SIP) modeling for ozone and regional haze. Currently available FEIs can differ by an order of magnitude (Li et al., 2020), so a well-developed FEI processing tool is essential to help understand the ranges of air quality impacts predicted using alternative FEIs by models such as the Comprehensive Air quality Model with extensions (CAMx). FEI processing is complex because the available inventories contain different information and omit some information needed by air quality models (e.g., daily temporal allocation, chemical speciation, and plume height profiles) requiring the use of supplementary data and assumptions. The TCEQ uses the Fire INventory from NCAR (FINN; Wiedinmyer et al., 2011) to estimate fire emissions,along with the Emissions Processing Software version 3 (EPS3) to prepare the FEI input to CAMx.

## 1.2 Project Objectives

The purpose of the project is to develop a literature-based tool to process various FEIs that could be used as a CAMx FEI input. The tool makes FEI comparisons more accessible and will improve the understanding of fire emissions impacts in exceptional event analyses and SIP modeling. Ramboll developed all necessary inputs (e.g., temporal, speciation, and plume height profiles) for fire emissions processing and created a user guide.

# 2.0 AVAILABLE FEI SUMMARY

We conducted a literature review to compile a list of available FEIs. FEIs use one of two different approaches: 1) burned area or 2) fire radiative power (FRP).

The burned area approach estimates fire emissions using estimated area burned from satellite measurements and assumptions of fuel consumption and vegetation-specific emission factors. FINN applies a burned area approach to estimate fire emissions using the following equation (Wiedinmyer et al., 2011; other burned area FEIs use similar equation):

$$E_i = A(x,t) \times B(x) \times FB \times ef_i$$

where the emission rate $E_i$ for chemical species $i$ is equal to the area burned at time $t$ and location $x$ $[A(x,t)]$ multiplied by the biomass loading at location $x$ $[B(x)]$, the fraction of that biomass that is burned in the fire $FB$, and the emission factor $ef_i$ (mass of species $i$ emitted per mass of biomass burned).

The FRP approach uses thermal anomalies from satellite measurements to measure the FRP, which is a rate of release of Fire Radiation Energy (FRE). The Moderate Resolution Imaging Spectroradiometer (MODIS) fire product suite[1] contains a variable for FRP, originally described in Kaufman et al. (1998), then revised by Giglio (2013) to account for varying pixel size across the detection swath. The equation used to calculate FRP is:

$$FRP = A_s \times \beta\left(T_f^8 - T_b^8\right)$$

where $T_f$ is the 4 micrometer (μm) brightness temperature of the fire pixel, $T_b$ is the mean 4 μm brightness temperature of the background window (averaged across a selection of nearby cloud-free land pixels that are not active fire pixels; Giglio et al., 2003), $A_s$ is the nominal MODIS pixel area evaluated at the scan angle $s$, and the coefficient β is equal to 4.34 x $10^{-19}$ W $m^{-2}$ $K^{-8}$. β is specific to the MODIS 4 μm spectral response. Freeborn et al. (2014) provide further information about MODIS FRP and quantifies uncertainties regarding use of FRP for active fire characterization and biomass burning estimation. FRP-based FEIs must then convert FRP to dry matter combustion rate, which depends on land cover characteristics (Kaiser et al., 2012). Finally, calculations of fire emissions by chemical species use land cover specific emissions factors applied to the dry matter combustion rates (Kasier et al., 2012).

Pan et al. (2020) provide global and regional comparisons of six FEIs and focus on aerosol emissions for 2008. The burned area FEIs analyzed by Pan et al. (2020) are:

- Global Fire Emissions Database version 3.1 (GFED3.1[2])
- GFED version 4 with small fires (GFED4s[3])
- FIre INventory from NCAR version 1.5 (FINN1.5[4])

[1] https://earthdata.nasa.gov/earth-observation-data/near-real-time/firms/active-fire-data

[2] https://daac.ornl.gov/VEGETATION/guides/global_fire_emissions_v3.1.html

[3] http://www.globalfiredata.org/

[4] http://bai.acom.ucar.edu/Data/fire/

while the FRP-based FEIs are:

- Global Fire Assimilation System version 1.2 (GFAS1.2[5])
- Fire Energetics and Emissions Research version 1.0 (FEER1.0[6])
- Quick Fire Emissions Dataset version 2.4 (QFED2.4[7])

Pan et al. (2020) found that while all FEIs showed similar spatial distributions, global total emissions for organic carbon (OC) and black carbon (BC) varied by factors of 3.7 and 3.4, respectively. Overall, burned area FEIs tended to show lower emissions compared to FRP-based FEIs. However, results varied widely across different regions.

Li et al. (2020) employed ensemble $PM_{2.5}$ forecasting using NOAA's Hybrid Single-Particle Lagrangian Integrated Trajectory model (HYSPLIT) applied to the November 2018 Camp Fire in Northern California using a matrix of meteorology inputs, plume rise schemes (Briggs, 1969; Sofiev et al., 2012), model setup options (mixing layer depths and vertical velocity) and these four FEIs (GFAS1.2 and FEER1.0 are the same as in Pan et al., 2020):

- GFAS1.2
- FEER1.0
- Global Biomass Burning Emissions Product from MODIS, Visible Infrared Imaging Radiometer Suite (VIIRS), and geostationary satellites (GBBEPx v2[8])
- Fire Locating and Monitoring of Burning Emissions-Arctic Research of the Composition of the Troposphere from Aircraft and Satellites (FLAMBE-ARCTAS[9])

Li et al. (2020) found a large variance in $PM_{2.5}$ concentrations among the 112 ensemble members, which at times exceeded 1,000 μg/m$^3$. This finding demonstrates the large uncertainties in wildfire forecasting, particularly regarding the source of FEIs.

Table 2-1 summarizes key characteristics of the available FEIs from both studies. All FEIs are available in near real-time (less than one day) unless otherwise noted. We present detailed descriptions of each FEI in the following section.

**Table 2-1. Summary of key characteristics of FEIs.**

| FEI dataset | Horizontal Resolution | Timeframe | Frequency | Approach | Burned Area/FRP Methodology | Emissions Species | Modeling Applications |
|---|---|---|---|---|---|---|---|
| FINN2.5 | 1 km$^2$ | 2002–2020 | Daily through 2020; previous calendar year available each July | Burned area | Estimated by active fire counts: 0.75 km$^2$ for savanna at each fire pixel, 1 km$^2$ for other types | NOx, VOC, CO, SO2, NH3, OC, $PM_{2.5}$ | FINN1.0: TCEQ NRTEEM (2017-2020); WACCM real time forecasts FINN2.2: TCEQ 2019 SIP modeling platform |

[5] https://apps.ecmwf.int/datasets/data/cams-gfas/

[6] http://feer.gsfc.nasa.gov/data/emissions/

[7] https://portal.nccs.nasa.gov/datashare/iesa/aerosol/emissions/QFED/v2.4r6/

[8] https://www.ospo.noaa.gov/Products/land/gbbepx/

[9] https://espo.nasa.gov/camp2ex/content/Global_Monitoring_and_Forecasting_of_Biomass-Burning_Smoke_Description_of_and_Lessons_From

| FEI dataset | Horizontal Resolution | Timeframe | Frequency | Approach | Burned Area/FRP Methodology | Emissions Species | Modeling Applications |
|---|---|---|---|---|---|---|---|
| GFED3.1 | 0.5°×0.5° | 2000–2012 | 3-hourly, daily, monthly | Burned area | MODIS | NOx, VOC, CO, SO2, NH3, OC, $PM_{2.5}$ | GEOS-Chem; MOZART |
| GFED4s | 0.25°×0.25° | 2000–2016 | 3-hourly, daily, monthly | Burned area | MODIS | NOx, VOC, CO, SO2, NH3, OC, BC, $PM_{2.5}$ | CMIP6 and AeroCom phase III experiments |
| BlueSky via EPA NEI | Data source dependent | EPA NEI years through 2019 | Hourly | Burned area | MODIS, HMS, other | NOx, VOC, CO, SO2, NH3, OC, BC, $PM_{2.5}$ | EPA NEI modeling platform |
| GFAS1.2 | 0.1°×0.1° | 2003–present | Daily | FRP | MODIS | NOx, VOC, CO, SO2, NH3, OC, BC, $PM_{2.5}$ | CAMS C-IFS |
| QFED2.5 | 0.1°×0.1° | 2000–Present | Daily with 1-month lag | FRP | MODIS | NOx, VOC, CO, SO2, OC, BC, $PM_{2.5}$ | GEOS-Chem; CAM-chem |
| FEER1.0 | 0.1°×0.1° | 2003–Present | Daily with 1-month lag | FRP | From GFASv1.2 (Kaiser et al., 2012) | NOx, VOC, CO, SO2, NH3, OC, BC, $PM_{2.5}$ | Fire research; climate impacts; Northern Sub-Saharan research |
| FLAMBE-ARCTAS | 0.1°×0.1° | 2000–present | Hourly, daily, monthly (unavailable as of Feb 2022) | FRP | MODIS, GOES | CO, $PM_{2.5}$, Total Carbon | NAAPS transport model |
| GBBEPx v3 | 0.1°×0.1° | Previous 2 days only | Daily, hourly | FRP | MODIS, VIIRS, GOES, Meteosat, MTSAT | CO, SO2, OC, BC, $PM_{2.5}$ | Operational global air quality forecasting with NEMS/GFS-GOCART; U.S. air quality forecasting with CMAQ |
| IS4FIRES | 0.1°×0.1° | 2000-present | 3-hourly | FRP | MODIS | $PM_{2.5}$ only | SILAM operated by FMI |

## 2.1 Burned Area FEIs

### 2.1.1 FINN2.5

The TCEQ uses FINN to estimate fire emissions for their SIP modeling. As of this writing (May 2022), FINN2.5 (released February 2022) is available through 2020. FINN2.5 has the highest 1 $km^2$ horizontal resolution.

Modeling projects originally performed in the Western U.S. by Western Regional Air Partnership/Western States Air Resources Council (WRAP/WESTAR) (and later adopted in TCEQ's SIP modeling) processed FINN fire emissions as point sources through Fortran-based preprocessors, creating Aerometric Information Retrieval System (AIRS) Facility Subsystem (AFS) files used as inputs to EPS3 modules designed to process FINN fires using temporal and vertical allocation schemes

developed by WRAP/WESTAR. According to the FINN website[10], NCAR plans to distribute FINN2.5 emissions as a global 0.1° gridded netCDF product. This format and structure will be consistent with the GFAS1.2 and QFED2.5 products. Currently, the FINN2.5 emissions product is only available as a CSV text file, where fire emissions are represented as points corresponding to the centers of MODIS and/or VIIRS satellite burn scar pixels. Rather than develop a new tool to bin the point-based emissions into a gridded product, we chose to use NCAR's existing Fortran-based tool to perform this function. We provide more information about this procedure in the User Guide.

### 2.1.2 GFED3.1

GFED3.1 uses the 500-m MODIS burned area product (Giglio et al., 2010) and fuel consumption per unit of burned area to determine the total dry matter consumed by biomass burning. Giglio et al. (2010) and van der Werf et al. (2010) detail fuel consumption characteristics used in GFED3.1. Calculation of emissions by chemical species use the amount of dry matter consumed multiplied by emission factors, which are developed in Andrae and Merlet (2001), Akagi et al. (2011) and other sources. GFED3.1 is available at 0.5° resolution and has been used in Model for Ozone and Related chemical Tracers (MOZART) and was the default FEI in GEOS-Chem prior to v10.01.

### 2.1.3 GFED4s

GFED4s contains updates to GFED3.1, including the addition of smaller fires as described in van der Werf et al. (2017) and revised fuel consumption characteristics using field campaign measurements (van Leeuwen et al., 2014). GFED4s is available at 0.25° resolution and has been used in many modeling applications, including GEOS-Chem (implemented in v10-01[11]), Coupled Model Intercomparison Project Phase 6 (CMIP6; Van Marle et al., 2017) and AeroCom phase III experiments[12].

### 2.1.4 SMARTFIREv2/BlueSky

The United States Environmental Protection Agency (EPA) uses the BlueSky modeling framework for the U.S. National Emissions Inventory (NEI) and prepares SMOKE-ready FF10 files for NEI years. At the time of this writing (February 2022), SMOKE-ready BlueSky fire emissions are available through 2019. The EPA uses Satellite Mapping Automatic Reanalysis Tools for Fire Incident Reconciliation version 2 (SMARTFIREv2) to produce inputs for BlueSky. Larkin and Raffuse (2015) and Larkin et al. (2009) describe BlueSky and SMARTFIRE as a "framework" for fire emissions modeling rather than a fire emissions model. SMARTFIREv2 relies on fire activity data sources that may not be available for months or years later[13]. Additionally, SMARTFIREv2 and BlueSky contain a menu of choices regarding fire activity datasets, weights, algorithms (SMARTFIREv2) as well as fuels, total consumption, time rate and emissions factors (BlueSky). Therefore, the SMARTFIREv2/BlueSky approach does not yield a consistent emissions product that can be easily evaluated against the other FEIs analyzed in this study.

## 2.2 FRP FEIs

### 2.2.1 GFAS1.2

GFAS multiplies FRP from MODIS Aqua/Terra satellite measurements by land cover specific conversion factors to obtain dry matter combustion rate estimates. GFAS then employs a sophisticated filtering

[10] https://www.acom.ucar.edu/Data/fire/

[11] http://wiki.seas.harvard.edu/geos-chem/index.php/GFED4_biomass_burning_emissions

[12] https://wiki.met.no/aerocom/phase3-experiments

[13] https://www3.epa.gov/ttnchie1/conference/ei20/session2/sraffuse_pres.pdf

system that masks spurious FRP signals from volcanoes, gas flaring and other industrial activity. GFAS includes vertical parameters – plume bottom, plume top and mean altitude of maximum injection height (described in Remy et al., 2017), all of which are derived from a plume rise model. GFAS also provides a separate injection height from IS4FIRES (Remy et al., 2017). As with the fire emissions, these vertical parameters have daily resolution which correspond to early afternoon. The European Centre for Medium-Range Forecasts (ECMWF) Composition Integrated Forecasting System (C-IFS) of Copernicus Atmospheric Monitoring Service (CAMS) utilizes GFAS1.2 for global real time fire and smoke forecasts. GFAS1.2 is available in near real-time at 0.1° resolution.

### 2.2.2 QFED2.5

Similar to GFAS, QFED uses FRP measurements from MODIS Aqua/Terra satellites. QFED calculates emissions using scaling factors applied to the FRP measurements. These scaling factors are developed from comparisons of aerosol optical depth (AOD) between NASA's Goddard Earth Observing System (GEOS) model and MODIS measurements across different regions (Darmenov and da Silva, 2015). QFED2.4 applies a sophisticated treatment of cloud obscured land areas and is used in NASA's NRT GEOS model and Modern-Era Retrospective analysis for Research and Applications version 2 (MERRA-2) reanalyses (Randles et al., 2017). NCAR's Community Atmosphere Model with chemistry (CAM-chem) also utilizes QFED and QFED is an optional FEI for GEOS-Chem. QFED2.4 emissions are available for the entire previous calendar month and have 0.1° resolution.

### 2.2.3 FEER1.0

FEER1.0 uses GFAS1.2 FRP data and multiplies by emission coefficients to obtain smoke aerosol emissions (Ichoku and Ellison, 2014). These emission coefficients were formulated from a detailed analysis of MODIS AOD and winds from NASA's MERRA reanalysis dataset (Rienecker et al., 2011). Scaling factors for chemical species including OC, BC, NOx, VOC, $SO_2$ and CO are then applied to the smoke aerosol emissions to obtain emissions for these species. Fire research, climate impacts and Northern Sub-Saharan research all utilize FEER emissions[14]. As with QFED, FEER emissions are available for the entire previous calendar month and have 0.1° resolution.

### 2.2.4 FLAMBE-ARCTAS

NASA, the U.S. Navy and NOAA originated the FLAMBE project to monitor fires and fire emissions globally. FLAMBE-ARCTAS utilizes FRP measurements from GOES in addition to MODIS (Reid et al., 2009). FLAMBE-ARCTAS uses empirical estimations of burned area for each satellite-detected fire and then applies factors for fuel loading/consumption and emission factors provided in Reid et al. (2005). Finally, the emissions are allocated temporally using an empirical diurnal cycle to produce hourly emissions of $PM_{2.5}$, CO and total carbon at 0.1° resolution. The Navy Aerosol Analysis and Prediction System (NAAPS) transport model uses FLAMBE-ARCTAS emissions. Unfortunately, FLAMBE-ARCTAS emissions are not publicly available at the time of this writing (February 2022).

### 2.2.5 GBBEPx v3

The GBBEPx emissions product is a blend of fire observations from QFED, VIIRS on the Suomi National Polar-orbiting Partnership (SNPP), GOES, Meteosat Second Generation satellites operated by the European Organization for the Exploitation of Meteorological Satellites (EUMETSAT), and the Multi-functional Transport Satellite (MTSAT) operated by the Japan Meteorological Agency (JMA). Operational global air quality forecasting with NOAA Environmental Modeling System-Global Forecasting System (NEMS-GFS) outfitted with the NASA Goddard Chemistry Aerosol Radiation and Transport Model (GOCART) aerosol model utilizes GBBEPx fire emissions (Zhang et al., 2019). In

[14] https://feer.gsfc.nasa.gov/data/emissions/

addition, GBBEPx emissions are used in NOAA Air Resources Laboratory (ARL) U.S. air quality forecasts using CMAQ. Version 3 of the dataset was recently released, superseding version 2 analyzed by Li et al. (2020). GBBEPx v3 is available at 0.1° resolution in near real-time only (historical emissions unavailable). The GBBEPx v3 product does not include NOx or VOC emissions.

### 2.2.6 IS4FIRES

The Finnish Meteorological Institute (FMI) developed the Integrated Monitoring and Modelling System for wildland fires (IS4FIRES) for integration into their global air quality forecasting model, System for Integrated modeLling of Atmospheric coMposition (SILAM). IS4FIRES uses MODIS FRP measurements along with emissions coefficients (Ichoku and Kaufman, 2005) and land cover specific scaling factors (Sofiev et al., 2009). IS4FIRES is available at 3-hourly intervals in near real-time at 0.1° resolution. However, only $PM_{2.5}$ emissions are currently available.

# 3.0 FEI SELECTION CRITERIA

We defined a set of criteria for selecting FEIs that may be useful for TCEQ exceptional event analyses and current SIP modeling as follows:

- Available in near real-time or maximum lag time of 1 month (for exceptional event analyses)
- Emissions for NOx, VOC and PM species
- 0.1 degree (~10 km) or better horizontal resolution
- Active use in the modeling community

Based on these criteria, we present our selection of two FEIs below. The chosen FEIs are compared to FINN2.5 in the following sections.

## 3.1 Final FEI Selection

Aside from FINN1.0, the only FEIs to meet all selection criteria outlined above are GFAS1.2, QFED2.5 and FEER1.0. FINN is a burned area FEI and the FINN1.0 emission estimation algorithm is presented earlier in this report. FINN2.5 will be fully documented in an upcoming publication (Wiedinmyer et al., in preparation). This version includes improvements to estimation of fire size, burned area and fuel loadings. Emission factors and VOC mapping are also updated from FINN1.0. Finally, FINN2.5 includes fire detections from VIIRS in addition to MODIS[15].

The vertical parameters provided by GFAS1.2 are a novel feature and a consideration for future FEI processor development. For this project, we wanted to keep the amount of customization specific to each FEI at a minimum. QFED2.5 and GFAS1.2 are both FRP FEIs and are similar regarding daily time resolution, 0.1° spatial resolution and emissions species. While QFED2.5 does not have the vertical information that GFAS1.2 has, it is in active use in the modeling community as an alternative to GFED4s in the GEOS-Chem model. QFED's sophisticated treatment of cloud obscured land areas could potentially improve emissions estimates relative to GFAS.

FEER1.0 is another FRP FEI similar product to QFED2.5, in terms of chemical species, format and temporal/spatial resolution. FEER's use of AOD to constrain emissions could warrant further investigation. However, we choose QFED2.5 over FEER1.0 due to more robust use in the modeling community (GEOS-Chem) and other models. FEER1.0 could be incorporated later due to its similarity to both GFAS1.2 and QFED2.5.

[15] https://www.acom.ucar.edu/Data/fire/

# 4.0 FEI TOOL PROCESSING STEPS

This section describes each of the FEI processing steps (regridding, chemical species mapping, temporal allocation, and vertical plume rise) in detail, as shown in the blue hatched box in Figure 4-1. Specific instructions for how to run the Python tool and execute necessary preprocessing steps are provided in the User Guide. The FEI processor provides output gridded emissions in CAMx-ready 3-D netCDF format.

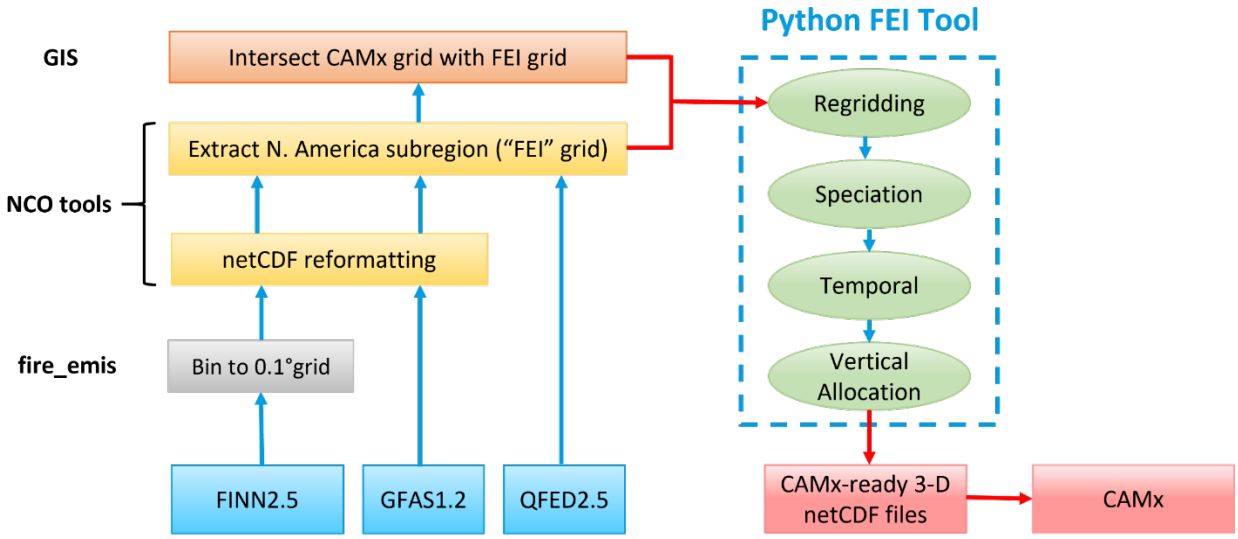


**Figure 4-1. Flow diagram for processing global gridded FEIs using the FEI processor.**

## 4.1 Regridding

The regridding step maps fire emissions from the 0.1° resolution "FEI grid" (spans +7.9° to +65° latitude and -150° to -40° longitude) to a target CAMx modeling grid using a cross-reference grid mapping file produced by a GIS intersection. The grid mapping file contains areas for each FEI grid cell that intersect each target CAMx grid cell. We provide instructions for performing this GIS intersection step in the User Guide. Because each FEI product contains emissions expressed as fluxes (emissions in kg $m^{-2}$ $s^{-1}$ or moles $m^{-2}$ $s^{-1}$), the regridding algorithm simply multiplies these fluxes by the FEI grid cell areas and sums them to obtain emission rate totals (kg $s^{-1}$ or moles $s^{-1}$) across each CAMx grid cell. As described earlier, we apply NCAR's existing Fortran-based tool (fire_emis) to bin the FINN point-based emissions into a gridded product. This program outputs emissions fluxes similar to the GFAS1.2 and QFED2.5 FEIs. We provide more information about this procedure in the User Guide. Because the FEI extent is common to the three FEIs used in this project, only one cross-reference file needs to be produced for each target CAMx domain. The output from this step creates gridded fire emissions for the target CAMx domain.

## 4.2 Chemical Species Mapping

After the regridding step, the FEI processor maps the available chemical species in the fire emissions file to the desired CAMx mechanism species. We provide the chemical species mapping for the initial May 2022 distribution of the FEI tool to CAMx CB6r4 (which works with the CAMx CB6r5 mechanism as well) from FINN2.5 in Table 4-1. We provide similar mapping tables for GFAS1.2 in

Table 4-2 and QFED2.5 in Table 4-3. We have provide these chemical species mappings as an input CSV file to the tool, which can be updated as needed. The MW column represents the molecular

weight of the FEI species to convert from mass to moles and a scale column that converts between the FEI species and CAMx species. All GFAS1.2 and QFED2.5 species (aerosols and gases) use emissions fluxes expressed in mass units, so molecular weights are applied to gases to convert from mass to moles for these two FEIs. FINN2.5 uses mass units for aerosols and moles for gases – therefore, we set the MW column to 1 for all species, including gases (see Table 4-1). The species mapping in each of the three tables utilize a more realistic (rapid) NOx to NOy conversion in smoke plumes, an approach obtained from the 2015 Texas Air Quality Research Program (AQRP) Fires project (McDonald-Buller et al., 2015). Additionally, all three mappings assume an organic mass to organic carbon (OM/OC) ratio of 1.

The CSV file also contains a comments column which we use to document any assumptions made about the FEI species. The FEI tool distribution contains mappings for the FINN1.0 product (available in near-real time) as well as a separate CSV file containing mappings for all four FEIs to the CAMx CB7 chemical mechanism. This processing step also converts the emission rate from $s^{-1}$ to $day^{-1}$, so that output from this step contains daily fire emissions for the target grid for all CAMx species.

**Table 4-1. Chemical species mapping from FINN2.5 to CAMx CB6r4 chemical mechanism.**

| CAMx Species | FINN2.5 Species | Scale | MW (g/mol) | Gas (G) or Aerosol (A) | Comment |
|---|---|---|---|---|---|
| PEC | BC | 1 | 1 | A | |
| FPRM | BC | -1 | 1 | A | |
| PAR | BIGALK | 5 | 1 | G | lumped alkanes C>3 |
| PAR | BIGENE | 0.5 | 1 | G | lumped alkenes C>3; used mapping from WACCM (0.5 IOLE 0.5 OLE 0.5 PAR) |
| OLE | BIGENE | 0.5 | 1 | G | lumped alkenes C>3; used mapping from WACCM (0.5 IOLE 0.5 OLE 0.5 PAR) |
| IOLE | BIGENE | 0.5 | 1 | G | lumped alkenes C>3; used mapping from WACCM (0.5 IOLE 0.5 OLE 0.5 PAR) |
| ETHY | C2H2 | 1 | 1 | G | |
| ETH | C2H4 | 1 | 1 | G | |
| ETOH | CH3CH2OH | 1 | 1 | G | |
| ETHA | C2H6 | 1 | 1 | G | |
| PAR | C3H6 | 1 | 1 | G | |
| OLE | C3H6 | 1 | 1 | G | |
| PRPA | C3H8 | 1 | 1 | G | |
| FORM | CH2O | 1 | 1 | G | |
| ALD2 | CH3CHO | 1 | 1 | G | |
| CH3CN | CH3CN | 1 | 1 | G | |
| ACET | CH3COCH3 | 1 | 1 | G | |
| MGLY | MGLY | 1 | 1 | G | |
| AACD | CH3COOH | 1 | 1 | G | acetic acid |
| MEOH | CH3OH | 1 | 1 | G | |
| ECH4 | CH4 | 1 | 1 | G | |
| CO | CO | 1 | 1 | G | |
| CRES | CRESOL | 1 | 1 | G | |
| GLYD | GLYALD | 1 | 1 | G | |

| CAMx Species | FINN2.5 Species | Scale | MW (g/mol) | Gas (G) or Aerosol (A) | Comment |
|---|---|---|---|---|---|
| HCN | HCN | 1 | 1 | G | |
| FACD | HCOOH | 1 | 1 | G | |
| PAR | HYAC | 2 | 1 | G | hydroxyacetone C3H6O2 |
| KET | HYAC | 1 | 1 | G | hydroxyacetone C3H6O2 |
| ISOP | ISOP | 1 | 1 | G | |
| ISPD | MACR | 1 | 1 | G | |
| PAR | MEK | 3 | 1 | G | |
| KET | MEK | 1 | 1 | G | |
| ISPD | MVK | 1 | 1 | G | |
| NH3 | NH3 | 1 | 1 | G | |
| NO | NO | 0 | 1 | G | mapping developed for AQRP FINN2.0 beta project |
| NO2 | NO | 0.736 | 1 | G | mapping developed for AQRP FINN2.0 beta project |
| PANX | NO | 0.008 | 1 | G | mapping developed for AQRP FINN2.0 beta project |
| NTR2 | NO | 0.02 | 1 | G | mapping developed for AQRP FINN2.0 beta project |
| HNO3 | NO | 0.18 | 1 | G | mapping developed for AQRP FINN2.0 beta project |
| NO | NO2 | 0 | 1 | G | mapping developed for AQRP FINN2.0 beta project |
| NO2 | NO2 | 0.736 | 1 | G | mapping developed for AQRP FINN2.0 beta project |
| PANX | NO2 | 0.008 | 1 | G | mapping developed for AQRP FINN2.0 beta project |
| NTR2 | NO2 | 0.02 | 1 | G | mapping developed for AQRP FINN2.0 beta project |
| HNO3 | NO2 | 0.18 | 1 | G | mapping developed for AQRP FINN2.0 beta project |
| POA | OC | 1 | 1 | A | |
| FPRM | OC | -1 | 1 | A | |
| CPRM | PM10 | 1 | 1 | A | |
| CPRM | PM25 | -1 | 1 | A | |
| FPRM | PM25 | 1 | 1 | A | |
| SO2 | SO2 | 1 | 1 | G | |
| TOL | TOLUENE | 1 | 1 | G | FINN2.5 maps toluene xylene and benzene explicitly |
| XYL | XYLENE | 1 | 1 | G | FINN2.5 maps toluene xylene and benzene explicitly |
| BENZ | BENZENE | 1 | 1 | G | FINN2.5 maps toluene xylene and benzene explicitly |
| OPEN | BZALD | 1 | 1 | G | benzaldehyde |
| TERP | APIN | 1 | 1 | G | |

| CAMx Species | FINN2.5 Species | Scale | MW (g/mol) | Gas (G) or Aerosol (A) | Comment |
|---|---|---|---|---|---|
| TERP | BPIN | 1 | 1 | G | |
| TERP | LIMON | 1 | 1 | G | |
| HONO | HONO | 1 | 1 | G | added in FINN2.5 |
| TERP | MYRC | 1 | 1 | G | myrcene |
| PAR | PHENOL | 1 | 1 | G | |
| UNR | PHENOL | 5 | 1 | G | dimethyl phenol from xylenes oxidation |
| TOL | XYLOL | 1 | 1 | G | dimethyl phenol from xylenes oxidation |
| PAR | XYLOL | 1 | 1 | G | dimethyl phenol from xylenes oxidation |

**Table 4-2. Chemical species mapping from GFAS1.2 to CAMx CB6r4 chemical mechanism.**

| CAMx Species | GFAS1.2 species | Scale | MW (g/mol) | Gas (G) or Aerosol (A) | Comment |
|---|---|---|---|---|---|
| CO | cofire | 1 | 28.01 | G | |
| ECH4 | ch4fire | 1 | 16.05 | G | |
| NO | noxfire | 0 | 46 | G | mapping developed for AQRP FINN2.0 beta project |
| NO2 | noxfire | 0.736 | 46 | G | mapping developed for AQRP FINN2.0 beta project |
| PANX | noxfire | 0.008 | 46 | G | mapping developed for AQRP FINN2.0 beta project |
| NTR2 | noxfire | 0.02 | 46 | G | mapping developed for AQRP FINN2.0 beta project |
| HNO3 | noxfire | 0.18 | 46 | G | mapping developed for AQRP FINN2.0 beta project |
| SO2 | so2fire | 1 | 64.04 | G | |
| MEOH | ch3ohfire | 1 | 32.05 | G | |
| ETOH | c2h5ohfire | 1 | 46.08 | G | |
| PRPA | c3h8fire | 1 | 44.11 | G | |
| ETH | c2h4fire | 1 | 28.05 | G | |
| PAR | c3h6fire | 1 | 42.09 | G | |
| OLE | c3h6fire | 1 | 42.09 | G | |
| ISOP | c5h8fire | 1 | 68.13 | G | |
| TERP | terpenesfire | 1 | 136.23 | G | assume MW 2*ISOP |
| FORM | ch2ofire | 1 | 30.03 | G | |
| ALD2 | c2h4ofire | 1 | 44.06 | G | |
| ACET | c3h6ofire | 1 | 58.09 | G | |
| NH3 | nh3fire | 1 | 17.04 | G | |
| DMS | c2h6sfire | 1 | 62.13 | G | |
| ETHA | c2h6fire | 1 | 30.08 | G | |
| TOL | c7h8fire | 1 | 92.15 | G | |
| BENZ | c6h6fire | 1 | 78.12 | G | |
| XYL | c8h10fire | 1 | 106.18 | G | |
| OLE | c4h8fire | 0.5 | 56.11 | G | assume 50/50 split between OLE/IOLE with PAR updated to reflect difference in carbon number |

| CAMx Species | GFAS1.2 species | Scale | MW (g/mol) | Gas (G) or Aerosol (A) | Comment |
|---|---|---|---|---|---|
| IOLE | c4h8fire | 0.5 | 56.11 | G | assume 50/50 split between OLE/IOLE with PAR updated to reflect difference in carbon number |
| PAR | c4h8fire | 1 | 56.11 | G | assume 50/50 split between OLE/IOLE with PAR updated to reflect difference in carbon number |
| OLE | c5h10fire | 0.5 | 70.13 | G | assume 50/50 split between OLE/IOLE with PAR updated to reflect difference in carbon number |
| IOLE | c5h10fire | 0.5 | 70.13 | G | assume 50/50 split between OLE/IOLE with PAR updated to reflect difference in carbon number |
| PAR | c5h10fire | 2 | 70.13 | G | assume 50/50 split between OLE/IOLE with PAR updated to reflect difference in carbon number |
| OLE | c6h12fire | 0.5 | 84.16 | G | assume 50/50 split between OLE/IOLE with PAR updated to reflect difference in carbon number |
| IOLE | c6h12fire | 0.5 | 84.16 | G | assume 50/50 split between OLE/IOLE with PAR updated to reflect difference in carbon number |
| PAR | c6h12fire | 3 | 84.16 | G | assume 50/50 split between OLE/IOLE with PAR updated to reflect difference in carbon number |
| OLE | c8h16fire | 0.5 | 112.21 | G | assume 50/50 split between OLE/IOLE with PAR updated to reflect difference in carbon number |
| IOLE | c8h16fire | 0.5 | 112.21 | G | assume 50/50 split between OLE/IOLE with PAR updated to reflect difference in carbon number |
| PAR | c8h16fire | 5 | 112.21 | G | assume 50/50 split between OLE/IOLE with PAR updated to reflect difference in carbon number |
| PAR | c4h10fire | 4 | 58.12 | G | |
| PAR | c5h12fire | 5 | 72.15 | G | |
| PAR | c6h14fire | 6 | 86.18 | G | |
| PAR | c7h16fire | 7 | 100.2 | G | |
| PEC | bcfire | 1 | 1 | A | |
| POA | ocfire | 1 | 1 | A | assume OC represents organic mass and not just organic carbon |
| FPRM | pm2p5fire | 1 | 1 | A | |
| FPRM | bcfire | -1 | 1 | A | |
| FPRM | ocfire | -1 | 1 | A | assume OC represents organic mass and not just organic carbon |
| CPRM | tpmfire | 1 | 1 | A | |
| CPRM | pm2p5fire | -1 | 1 | A | |

**Table 4-3. Chemical species mapping from QFED2.5 to CAMx CB6r4 chemical mechanism.**

| CAMx Species | QFED2.5 species | Scale | MW (g/mol) | Gas (G) or Aerosol (A) | Comment |
|---|---|---|---|---|---|
| ACET | ACET | 1 | 58.09 | G | |
| ALD2 | ALD2 | 1 | 44.06 | G | |
| PAR | ALK4 | 5 | 72.15 | G | assume pentane for consistency with BIGALK in FINN |
| ETHA | C2H6 | 1 | 30.08 | G | |
| PAR | C3H6 | 1 | 42.09 | G | |
| OLE | C3H6 | 1 | 42.09 | G | |
| PRPA | C3H8 | 1 | 44.11 | G | |
| FORM | CH2O | 1 | 30.03 | G | |
| ECH4 | CH4 | 1 | 16.05 | G | |
| CO | CO | 1 | 28.01 | G | |
| PAR | MEK | 3 | 72.11 | G | |
| KET | MEK | 1 | 72.11 | G | |
| NH3 | NH3 | 1 | 17.04 | G | |
| NO | NO | 0 | 30.01 | G | mapping developed for AQRP FINN2.0 beta project |
| NO2 | NO | 0.736 | 30.01 | G | mapping developed for AQRP FINN2.0 beta project |
| PANX | NO | 0.008 | 30.01 | G | mapping developed for AQRP FINN2.0 beta project |
| NTR2 | NO | 0.02 | 30.01 | G | mapping developed for AQRP FINN2.0 beta project |
| HNO3 | NO | 0.18 | 30.01 | G | mapping developed for AQRP FINN2.0 beta project |
| SO2 | SO2 | 1 | 64.04 | G | |
| PEC | BC | 1 | 1 | A | |
| POA | OC | 1 | 1 | A | assume OC represents organic mass and not just organic carbon |
| FPRM | PM25 | 1 | 1 | A | |
| FPRM | BC | -1 | 1 | A | |
| FPRM | OC | -1 | 1 | A | assume OC represents organic mass and not just organic carbon |

## 4.3 Temporal Allocation

Next, the FEI processor distributes the daily total emissions to individual hours via a temporal profile. Figure 4-2 (reproduced from Ramboll Environ; 2016), shows prescribed (RX_count; shown in red) and wildfire (WF_count; shown in blue) diurnal temporal profiles developed by the EPA based on GOES East and West satellite detects using the 2012-2014 NOAA's Hazard Mapping System (HMS) daily fire data diurnal profiles. For comparison, we show the WRAP-Fire Emissions Joint Forum (WRAP-FEJF; shown in green) diurnal profile used for both wildfires and prescribed fires (Air Sciences Inc., 2004). Modeling projects originally performed in the Western U.S. by WRAP/WESTAR (and later adopted in TCEQ's SIP modeling) allocated daily FINN fire emissions throughout the day using this WRAP-FEJF diurnal profile. Ramboll Environ (2016) noted: "*the EPA wildfire profile shows "false detail" that may be related to how the composite profile is constructed. EPA should consider smoothing the wildfire profile. A hypothesis that the midday dip in wildfire counts could be due to dampening by summer afternoon rainstorms probably does not apply to many fires in the West, and further suggests a large*

*or disproportionate eastern US weighting in the composite. It may also be possible that satellite detects are affected by interference from deep afternoon cloudiness."*

Figure **4-2** also shows the single diurnal temporal profile that is currently used by the FEI processor (shown in green). This profile attempts to smooth some of the "false detail" that may be present in both the EPA and WRAP-FEJF profiles. Additionally, since we do not have a way to determine fire type (prescribed or wildfire) from the gridded FEI products, we developed the profile to be used for all fire types. The FEI processor reads in the temporal profile as a CSV text file, so adjustments could easily be implemented. We recommend literature review to investigate and test alternative temporal profiles for future work.

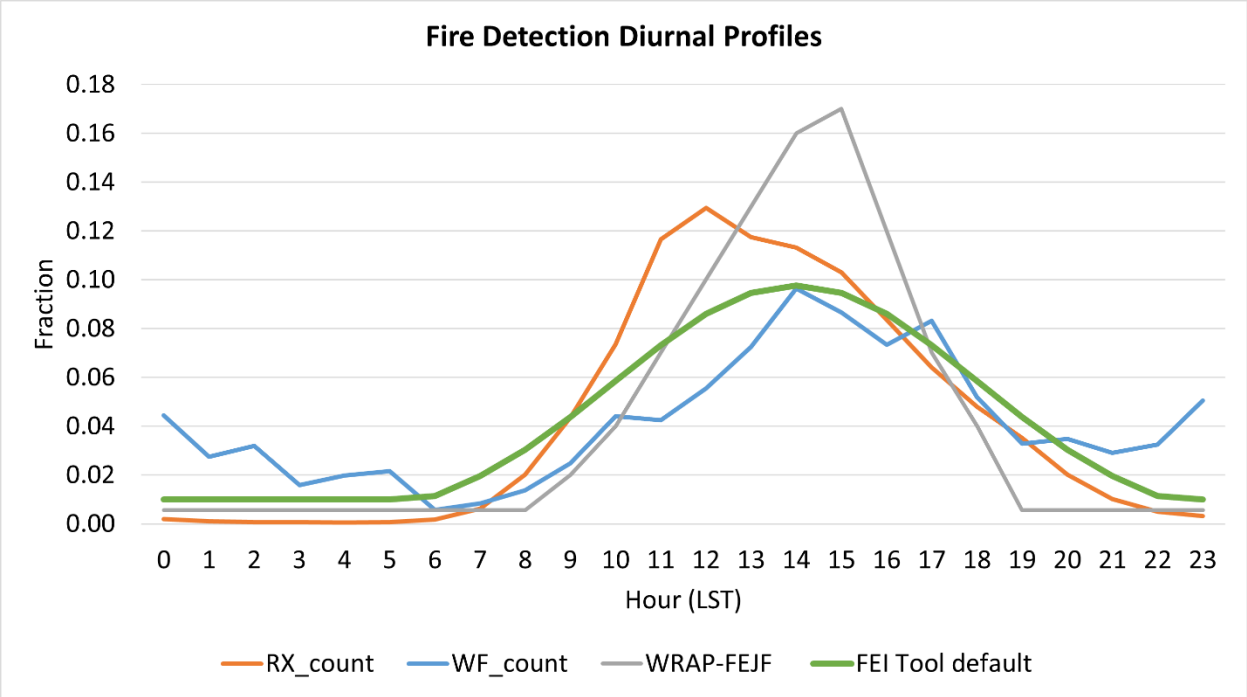


**Figure 4-2. Diurnal profiles of fire counts from GOES satellite for prescribed (RX_count; orange) and wildfires (WF_count; blue), diurnal emission profile from WRAP-FEJF (Air Sciences Inc., 2004; grey), and default diurnal profile used by the FEI processor (green).**

### 4.4 Vertical Allocation

The final step in the FEI processing allocates hourly fire emissions vertically. After reviewing plume rise algorithms (Sofiev et al., 2012; Ramboll Environ, 2016; Wilkins et al., 2022) and taking into consideration the lack of necessary information, we decided to apply the PBL500 plume rise algorithm with adaptations to distribute emissions vertically between the ground surface and plume top. Wilkins et al. (2022) defines the PBL500 plume injection height as simply the planetary boundary layer (PBL) height plus 500 m. The authors then compare SMOKE-Briggs smoke plume injection heights against those from PBL500 and another plume rise algorithm, Sofiev, as described in Sofiev et al. (2012) for several different days during the 2013 California Rim Fire and 2017 prescribed burns in Kansas using Cloud-Aerosol Lidar with Orthogonal Polarization (CALIOP) satellite measurements. The paper shows evidence that plume injection heights from the PBL500 scheme are comparable or in some cases better than those from the Sofiev scheme.

The PBL500 plume rise algorithm (as well as Sofiev) predict only the injection height or top of the smoke plume. We therefore developed a methodology similar to that used in the SMOKE-Briggs approach, where we: 1) define the ground surface as the bottom of the smoke plume; 2) allocate 90% of the total column hourly emissions to the top 2/3 of the plume; and 3) allocate the remaining 10% of emissions to the bottom 1/3 of the plume. We distribute emissions in each CAMx model layer weighted by layer thickness. Figure 4-3 shows an example vertical profile for a grid cell with a PBL height of 2,000 m and 100 mol of total column CO emissions.

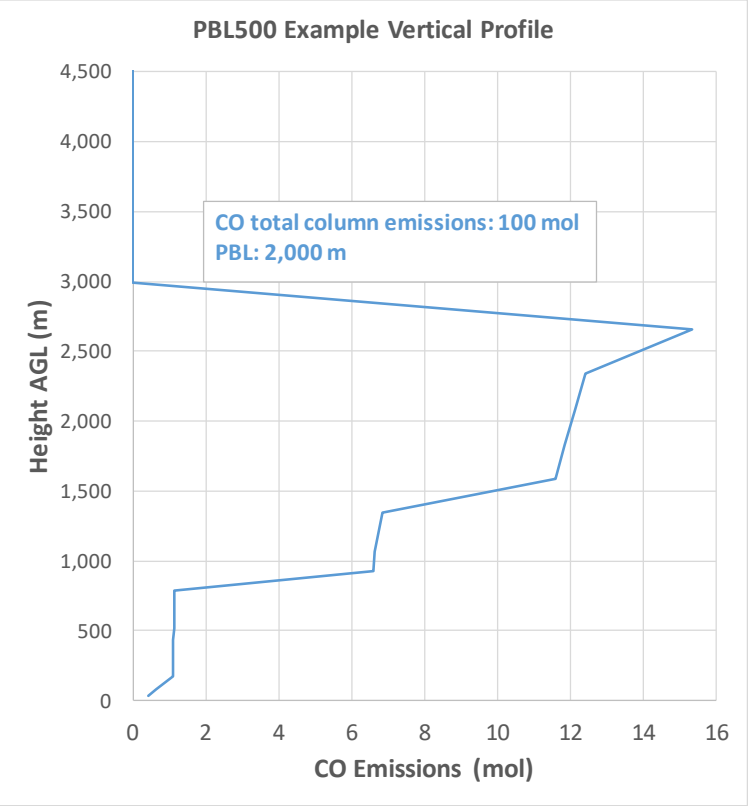


**Figure 4-3. PBL500 example vertical profile showing vertical distribution of emissions where the total column CO emissions are 100 moles and PBL height is 2,000 m.**

We also considered the Sofiev plume rise algorithm for the FEI processor. Sofiev et al. (2012) derived an energy-balance parameterization of plume injection height that accounts for PBL mixing, power law dependence of fire intensity, and stability in the free troposphere. The Sofiev scheme includes 4 fitted tunable parameters to match observed plume heights by NASA's Multi-angle Imaging SpectroRadiometer (MISR). We provide the equation and definition of variables below:

$$H_P = \alpha H_{PBL} + \beta \left(\frac{FRP}{P_{f0}}\right)^{\gamma} \exp\left(-\delta N_{FT}^2 / N_0^2\right)$$

where $H_P$ is height of plume top; $H_{PBL}$ is PBL height; *FRP* is fire radiative power; $P_{f0}$ is reference fire power; $P_{f0}$ = $10^6$ W; $N_0$ is the reference Brunt-Väisälä frequency; $N_0^2$ = $2.5\times10^{-4}$ $s^{-2}$; $N_{FT}$ is the Brunt-Väisälä frequency; $\alpha$ is the fraction of PBL passed freely; $\alpha < 1$; $\beta$ is the weight of fire intensity contribution ($\beta > 0\ m$); $\gamma$ is the power of dependence on FRP; $\gamma < 0.5$; $\delta$ is the weight of dependence on

free troposphere stability ($\delta \geq 0$). The scheme provides two alternative ways of setting the $\alpha, \beta, \gamma, \delta$ parameters:

(1) one-stage: $\alpha = 0.24;\ \beta = 170m;\ \gamma = 0.35;\ \delta = 0.6$

(2) two-stage:

stage 1:

$\alpha = 0.15;\ \beta = 102\ m;\ \gamma = 0.49;\ \delta = 0$

stage 2:

$\alpha = 0.24;\ \beta = 170\ m;\ \gamma = 0.35;\ \delta = 0.6\ (H_P \leq H_{pbl})$

$\alpha = 0.93;\ \beta = 298\ m;\ \gamma = 0.13;\ \delta = 0.7\ (H_P > H_{pbl})$

$N_{FT}$ can be derived from potential temperature ($\theta$):

$$N_{FT} = \sqrt{\frac{g}{\theta}\frac{d\theta}{dz}}\ (z \approx 2H_{PBL})$$

The Sofiev parameterization therefore requires FRP, Brunt-Väisälä frequency ($N_{FT}$) and PBL height ($H_{PBL}$). While $N_{FT}$ and $H_{PBL}$ can be calculated from WRFCAMx variables, GFAS1.2 is the only FEI that includes FRP. We therefore decided to explore the relationship between GFAS1.2 FRP and CO emissions fluxes. Examination of this relationship by month (see Figure 4-4) revealed distinct linear regression slopes which appear to correspond to landcover-specific fuel types used by the GFAS system. These scatter plots divide the U.S. into Western (left panels) and Eastern (right panels) regions using -104° longitude and show daily FRP and CO emission fluxes for individual 0.1° grid cells. In general, the Eastern U.S. plots show more diversity, reflecting different fuel characteristics where fires are active. The much larger values for FRP (near 200 W $m^{-2}$) in the September 2020 Western U.S. plot (bottom left panel) reflect the numerous intense Western wildfires observed during this period. For future work, we recommend implementing and testing the Sofiev plume rise algorithm using monthly CO/FRP factors to obtain FRP for non-GFAS FEIs.

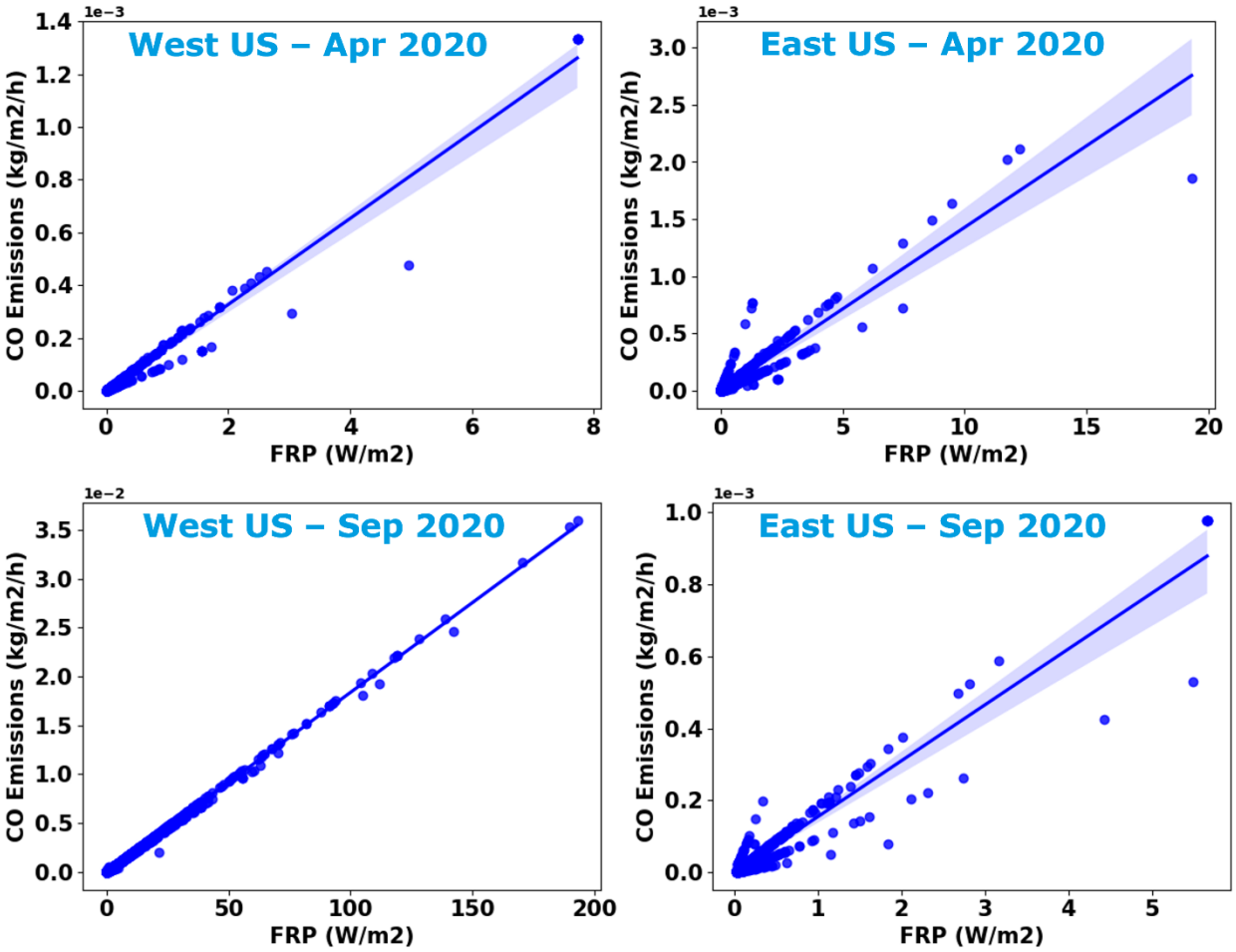


**Figure 4-4. Monthly scatter plots showing daily FRP (W $m^{-2}$) vs. CO emissions fluxes (kg $m^{-2}$ $hr^{-1}$) for the Western US in April 2020 (top left), Eastern US in April 2020 (top right), Western US in September 2020 (bottom left) and Eastern US in September 2020 (bottom right).**

# 5.0 COMPARISON OF FEIS

In this section, we compare emissions from FINN2.5, QFED2.5, and GFAS1.2 for (1) the 2019 ozone season in section 5.1 and (2) two days when fires impacted ozone concentrations in Texas that were modeled by the NRTEEM system in section 5.2.

## 5.1 2019 Ozone Season

After processing the FINN2.5, GFAS1.2, and QFED2.5 fire emissions through the FEI processor for the North America 36US3 domain, we compiled emission summaries for the 2019 ozone season (April 1 – October 31, 2019). Table 5-1 and Table 5-2 present these summaries for total $PM_{2.5}$ and NOx, VOC and CO emissions for several U.S. states including Texas, respectively. We selected California, Oregon and Washington because these states typically have numerous, large wildfires that can transport ozone and $PM_{2.5}$ to Texas. We selected several additional states surrounding Texas where agricultural burning is common in the Spring and/or Fall. In general, the emissions summaries show considerable variation among the FEIs, which agrees with our analysis for individual days presented in Section 5.2. As described earlier, each FEI product processes the raw satellite measurements differently and each of these processes carry some degree of uncertainty, often resulting in significant differences in the number/size of identified fires and associated emission estimates.

Except for California VOC emissions, QFED2.5 has higher emissions than GFAS1.2 across all states and key pollutants. QFED2.5 $PM_{2.5}$ emissions are highest among the three FEIs for all states shown in Table 5-1, including Texas (QFED2.5 $PM_{2.5}$ emissions nearly 3 times higher than FINN2.5 and over six times higher than GFAS1.2 across Texas). GFAS1.2 $PM_{2.5}$ emissions are lowest among the three FEIs with the single exception of Kansas. NOx emissions show better agreement than $PM_{2.5}$ emissions, particularly between FINN2.5 and QFED2.5. As with $PM_{2.5}$ emissions, GFAS1.2 has the lowest NOx emissions among the three FEIs for each of the states shown in Table 5-1. FINN2.5 VOC emissions (see Table 5-2) are considerably larger than both GFAS1.2 (about 13 times greater in Texas) and QFED2.5 (about 7 times greater in Texas). We provide emission totals for all U.S. states in Appendix A.

**Table 5-1. $PM_{2.5}$ and NOx Emissions summaries for FINN2.5, GFAS1.2 and QFED2.5 for April 1 – October 31, 2019 for selected U.S. states.**

| | $PM_{2.5}$ (tons) | | | NOx (tons) | | |
|---|---|---|---|---|---|---|
| **State** | **FINN2.5** | **GFAS1.2** | **QFED2.5** | **FINN2.5** | **GFAS1.2** | **QFED2.5** |
| California | 55,106 | 40,724 | 180,636 | 14,406 | 10,106 | 23,871 |
| Oregon | 77,744 | 13,267 | 112,418 | 15,186 | 2,874 | 9,645 |
| Washington | 42,302 | 13,947 | 86,569 | 9,054 | 3,044 | 10,884 |
| Oklahoma | 12,896 | 7,421 | 35,290 | 5,562 | 1,990 | 10,287 |
| Kansas | 9,594 | 14,765 | 52,629 | 6,060 | 4,286 | 21,948 |
| Arkansas | 29,441 | 4,674 | 45,369 | 8,774 | 755 | 8,290 |
| Louisiana | 36,631 | 7,492 | 70,342 | 9,129 | 1,459 | 7,504 |
| Texas | 33,311 | 14,820 | 95,027 | 11,487 | 3,559 | 18,040 |

**Table 5-2. VOC and CO Emissions summaries for FINN2.5, GFAS1.2 and QFED2.5 for April 1 – October 31, 2019 for selected U.S. states.**

| | VOC (tons) | | | CO (tons) | | |
|---|---|---|---|---|---|---|
| **State** | **FINN2.5** | **GFAS1.2** | **QFED2.5** | **FINN2.5** | **GFAS1.2** | **QFED2.5** |
| California | 221,797 | 45,544 | 33,999 | 411,136 | 424,232 | 495,357 |
| Oregon | 271,103 | 11,350 | 17,828 | 525,544 | 125,029 | 244,181 |
| Washington | 157,568 | 13,307 | 15,938 | 297,209 | 131,955 | 230,556 |
| Oklahoma | 62,028 | 6,743 | 10,237 | 113,186 | 91,609 | 165,953 |
| Kansas | 58,161 | 14,725 | 19,488 | 96,901 | 185,386 | 328,749 |
| Arkansas | 163,814 | 3,514 | 10,006 | 276,381 | 51,000 | 152,635 |
| Louisiana | 173,255 | 5,249 | 12,095 | 315,359 | 73,877 | 170,861 |
| Texas | 148,615 | 11,386 | 21,390 | 282,219 | 170,429 | 328,035 |

## 5.2 Case Studies

Next, we compare FEIs for two days when fires impacted ozone concentrations in Texas that were modeled by the NRTEEM system:

- April 9, 2019
- October 8, 2020

### 5.2.1 NRTEEM Background

At the end of each ozone season, Ramboll analyzed high ozone events where the NRTEEM system modeled substantial impacts from wildfires. We present summaries of two such events from April 9, 2019 and October 8, 2020, adapted from NRTEEM final reports (Johnson et al., 2019; Ramboll,

2020). We then present graphical and tabular FEI comparisons for these events. No new modeling was conducted for this analysis.

From 2013 to 2016, Ramboll operated an NRT daily ozone forecasting system for the TCEQ (Johnson et al., 2016). In 2017, Ramboll leveraged the NRT system to develop the Fire Impact Modeling (FIM) system. FIM demonstrated usefulness by identifying potential days when exceptional events may be responsible for ozone exceedances (Johnson et al., 2017). From 2018-2020, we developed and deployed the NRTEEM system that expanded upon the FIM system by adding two new potential sources of exceptional events: 1) stratospheric ozone intrusion and 2) Mexican anthropogenic emissions (Johnson et al., 2018).

In addition to identifying potential exceptional events and estimating Clean Air Act §179B international emissions impacts, running WRF and CAMx daily provides insights into ozone formation in Texas and VOC/NOx emissions sensitivity. While in operation, the TCEQ makes continual improvements to the NRTEEM system to make it more useful. NRTEEM ozone results have been distributed in near real-time on a TCEQ website while the NRTEEM system is in operation.

### 5.2.2 April 9, 2019

On April 9, 2019, the Longview CAMS 19 and Tyler CAMS 82 monitoring sites in the Tyler-Longview-Marshall area of Northeast Texas recorded maximum daily 8-hour (MDA8) ozone values exceeding 70 ppb. The April 9 MDA8 ozone values were the highest recorded in 2019 at these sites (Table 5-3).

**Table 5-3. Dates and MDA8 ozone on the four highest ozone days of 2019 at Tyler-Longview-Marshall area CAMS sites (from TCEQ website accessed on February 10, 2022).**

| Site | Date | 1st Highest MDA8 Ozone (ppb) | Date | 2nd Highest MDA8 Ozone (ppb) | Date | 3rd Highest MDA8 Ozone (ppb) | Date | 4th Highest MDA8 Ozone (ppb) |
|---|---|---|---|---|---|---|---|---|
| Longview C19 | 4/9/2019 | 74 | 5/13/2019 | 69 | 9/6/2019 | 68 | 8/15/2019 | 67 |
| Tyler Airport Relocated C82 | 4/9/2019 | 80 | 8/15/2019 | 68 | 4/15/2019 | 67 | 4/10/2019 | 67 |
| Karnack C85 | 5/15/2019 | 67 | 9/7/2019 | 66 | 9/6/2019 | 64 | 4/27/2019 | 62 |

NOAA's Descriptive Text Narrative for Smoke/Dust Observed in Satellite Imagery[16] noted the presence of fires from agricultural burns in Texas, Oklahoma and Kansas (Figure 5-1). Areas of smoke were diagnosed by NOAA analysts using GOES-East and GOES-West visible satellite imagery.

[16] https://www.ready.noaa.gov/data/archives/fires/national/arcweb/20190409/discuss01.txt

**Tuesday, April 9, 2019**

DESCRIPTIVE TEXT NARRATIVE FOR SMOKE/DUST OBSERVED IN SATELLITE IMAGERY
THROUGH 1800Z April 9, 2019

SMOKE:
Central/Southern Plains...
Numerous agricultural fires were seen across north Texas, Oklahoma, and
eastern Kansas through the morning. These fires were producing plumes
of mainly light-density smoke. Individual plume motion was primarily
northward in Texas and Oklahoma, and northwestward in Kansas. In addition,
a large area of remnant smoke from yesterday's fires in the same areas
extended from southeastern Kansas southward across east Texas to the
Gulf of Mexico. This area consisted of up to moderate-density smoke and
was drifting slowly southward

**Figure 5-1. NOAA discussion of smoke in satellite imagery from April 9, 2019.**

The NOAA Hazard Mapping System (HMS) fire detection and smoke product for April 9 (upper right panel of Figure 5-2) shows many fires burning in Texas, Oklahoma and eastern Kansas and a plume of smoke extending from the fires southward into Northeast Texas. Only one image is available for each day from HMS, so we accessed GOES satellite products, which are available throughout the day. The smoke plume from the fires is apparent as an area of enhanced AOD in the GOES-16 AOD retrieval (lower right panel of Figure 5-2) and aligns fairly well with the HMS smoke product. Note that the AOD cannot be retrieved for areas that are covered by clouds. The NRTEEM PM fine smoke tracer for the same hour (11 am CST) as the GOES-16 AOD image simulates a plume that corresponds reasonably well with the GOES-16 AOD retrieval. NRTEEM shows an impact on MDA8 ozone values that exceeds 5 ppb in Northeast Texas and the Dallas-Fort Worth area and exceeds 2 ppb in Houston.

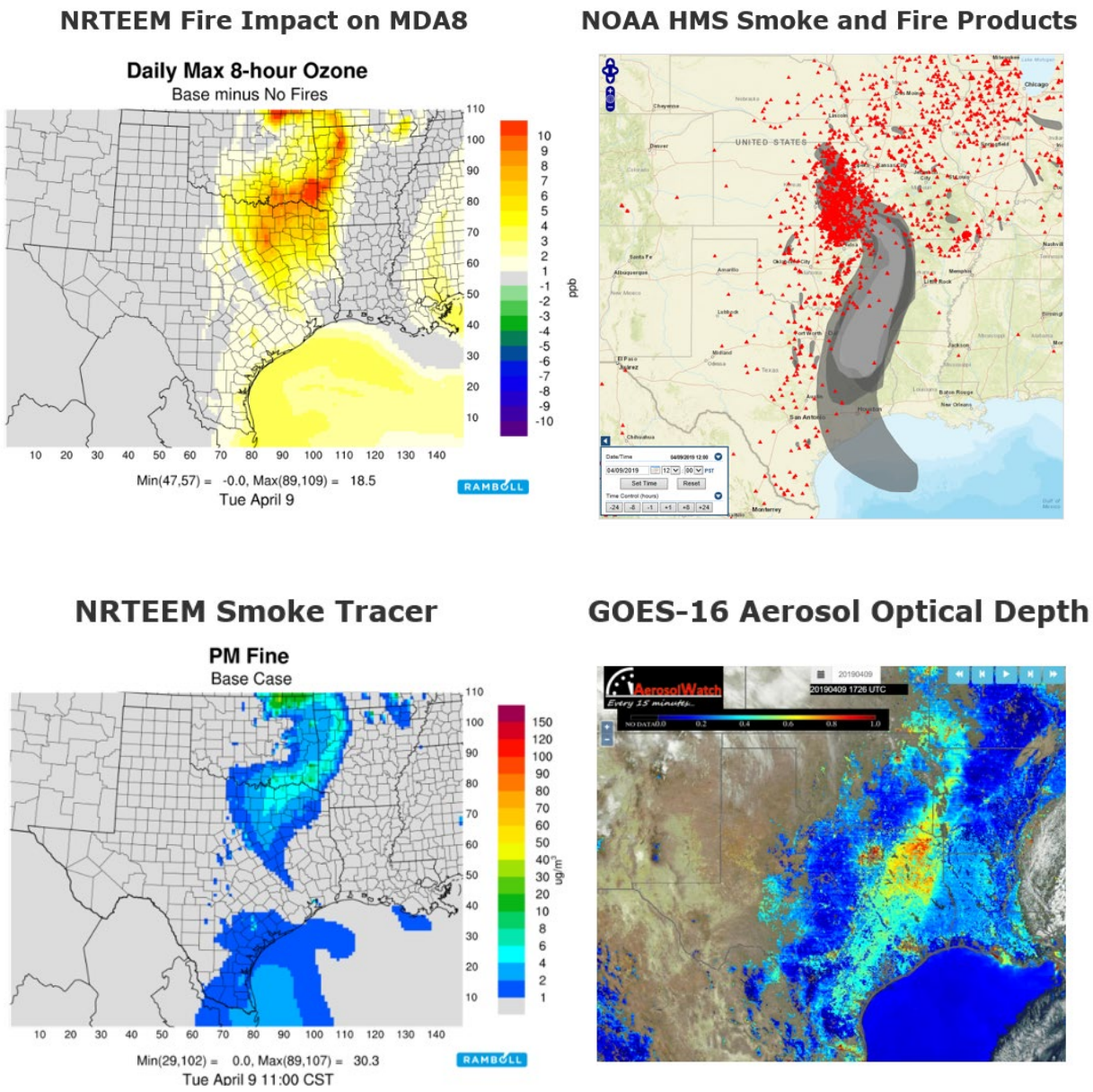


**Figure 5-2. Upper left: NRTEEM modeled fire impacts on MDA8 ozone. Upper right: NOAA satellite fire detections (red triangles) and diagnosed smoke (grey image developed using online tools at Airnowtech.org). Lower left: NRTEEM modeled 1-hour average $PM_{2.5}$ at 11 AM CST. Lower right: GOES-16 AOD retrieval for 11:26 AM CST (image from NOAA's AerosolWatch website[17])**

17 https://www.star.nesdis.noaa.gov/smcd/spb/aq/AerosolWatch/?product_date=20190409&zoom=5&lat0=37.00000000000003&lon0=-95&layers=1&region=conus

#### 5.2.2.1 Graphical Comparison of $PM_{2.5}$ Emissions

Figure 5-3 shows the satellite fire detections (red triangles) and NOAA HMS diagnosed smoke on April 9, 2019. The approximate extent for our FEI comparison is shown in blue. Figure 5-4 presents spatial maps of daily total $PM_{2.5}$ emissions on April 9, 2019 for FINN2.5 (left), GFAS1.2 (middle) and QFED2.5 (right). We processed each of these three FEIs through the FEI processor and extracted the same subregion for each. The spatial patterns for all three FEIs look similar, but the magnitudes are quite different. The FINN2.5 emissions (left panel of Figure 5-4) show a domain-wide maximum of 61.2 tons per day (tpd) with varying magnitudes across the domain. The GFAS1.2 emissions (middle panel of Figure 5 4) show fewer detected fires but considerable variation, with many grid cells under 2 tpd and a domain-wide max of 243 tpd. The QFED2.5 emissions (right panel of Figure 5-4) show even fewer fire detections than GFAS1.2, but with more variation than either FINN2.5 or GFAS1.2, from less than 1 to over 400 tpd.

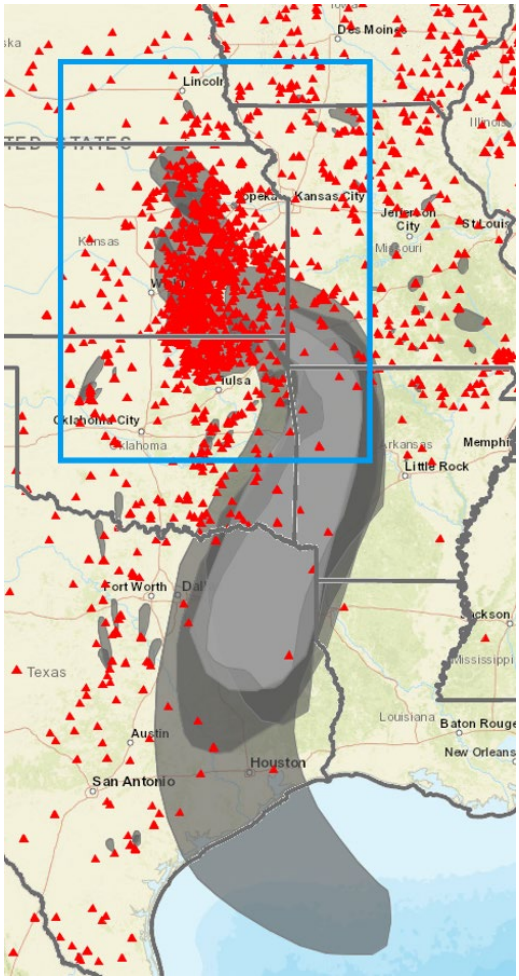


**Figure 5-3. NOAA satellite fire detections (red triangles) and diagnosed smoke on April 9, 2019 (image developed using online tools at airnowtech.org). The approximate spatial extent for the FEI comparison in Figure 5-4 is shown in blue.**

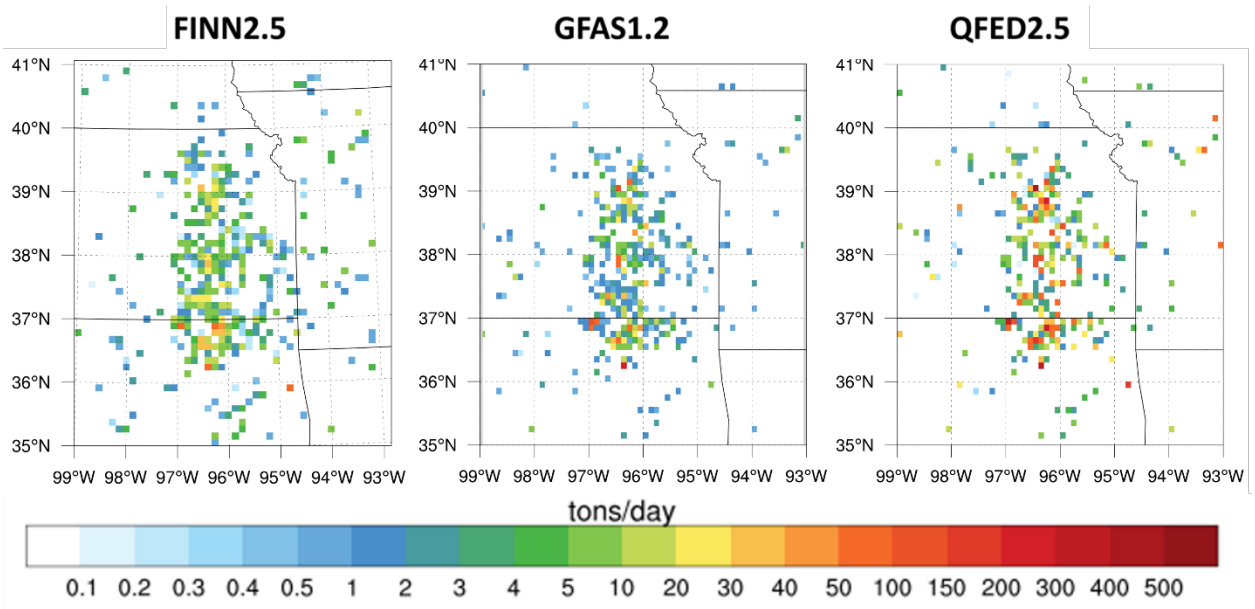


**Figure 5-4. Daily total $PM_{2.5}$ fire emissions (tons/day) for FINN2.5 (left), GFAS1.2 (middle) and QFED2.5 (right) on April 9, 2019.**

#### 5.2.2.2 Emissions Summaries

Table 5-4 presents daily total NOx, VOC, $PM_{2.5}$ and CO emissions for FINN2.5, GFAS1.2 and QFED2.5 over the area shown in Figure 5-4. While CO emissions across the three FEIs are all within a factor of 2, QFED2.5 $PM_{2.5}$ emissions are over 3.2 times higher than FINN2.5 and 2.9 times higher than GFAS1.2. VOC emissions show the worst agreement across the three FEIs, with FINN2.5 VOC emissions 4.3 times greater than GFAS1.2 and 6.3 times greater than QFED2.5.

**Table 5-4. Emissions summaries for FINN2.5, GFAS1.2 and QFED2.5 on April 9, 2019. Spatial extent of area comparison is shown in Figure 5-3.**

| | Emissions (tons/day) | | |
|---|---|---|---|
| **Species** | **FINN2.5** | **GFAS1.2** | **QFED2.5** |
| NOx | 1,360 | 686 | 2,587 |
| VOC | 10,944 | 2,507 | 1,730 |
| $PM_{2.5}$ | 2,098 | 2,354 | 6,756 |
| CO | 19,943 | 28,829 | 39,911 |

### 5.2.3 October 8, 2020

On October 8, 2020, the Denton Airport South CAMS 56 monitor in Dallas-Fort Worth (DFW) recorded an MDA8 ozone value of 71 ppb, which was the highest value of any monitor in the area. The NRTEEM wildfire contribution to MDA8 ozone at CAMS 56 was 5.5 ppb, which was the highest wildfire contribution at any Texas CAMS site in 2020 and was the fourth highest MDA8 value of 2020 for CAMS 56[18].

[18] https://www.tceq.texas.gov/cgi-bin/compliance/monops/8hr_4highest.pl

The TCEQ's Daily Air Quality Forecast Update for October 8 predicted, "*Light to moderate amounts of smoke from wildfires in Colorado and Wyoming may continue lingering over the Texas Panhandle through the Permian Basin while expanding into Far West Texas and the Rio Grande Valley, though much of the smoke may remain aloft. Meanwhile, the light to moderate amounts of smoke from seasonal fires across portions of East Texas and the Southeast U.S. may linger over the eastern two-thirds of the state as well*."

The NRTEEM MDA8 ozone map for October 8 (left panel of Figure 5-5) shows a broad swath of wildfire impacts across Texas and surrounding states. In Figure 5-6, we present ozone time series for August 5-8 at CAMS 58 (observations as black dotted line; base model as blue line; No Fires scenario as black line). The base model generally simulated ozone well during this period. The model underestimated peak 1-hour ozone on August 8 by 7 ppb and showed a maximum 1-hour average ozone impact from wildfires of 6 ppb.

To explore potential source-receptor relationships between wildfires and ozone at CAMS 58 on October 8, we developed back trajectories using HYSPLIT. We used online tools on NOAA ARL's Real-time Environmental Applications and Display sYstem (READY) website (Rolph, 2017) to develop back trajectories with three-dimensional gridded weather data provided by the North American Model (NAM). The NAM has spatial resolution 12 km. As shown in the right panel of Figure 5-5, back trajectories originating above CAMS 58 have curved paths which indicate shifting winds in the period leading up to October 8. From October 5-6, air originating in the Colorado-Nebraska-Kansas region travelled southeast toward the DFW area. By October 7, the wind shifted so that the trajectories began turning clockwise and by October 8 winds in the DFW area were from the southeast as Hurricane Delta drew near. The HYSPLIT back trajectories indicate the potential for this smoke-affected air mass over the Central Plains states to have influenced air in DFW on October 8.

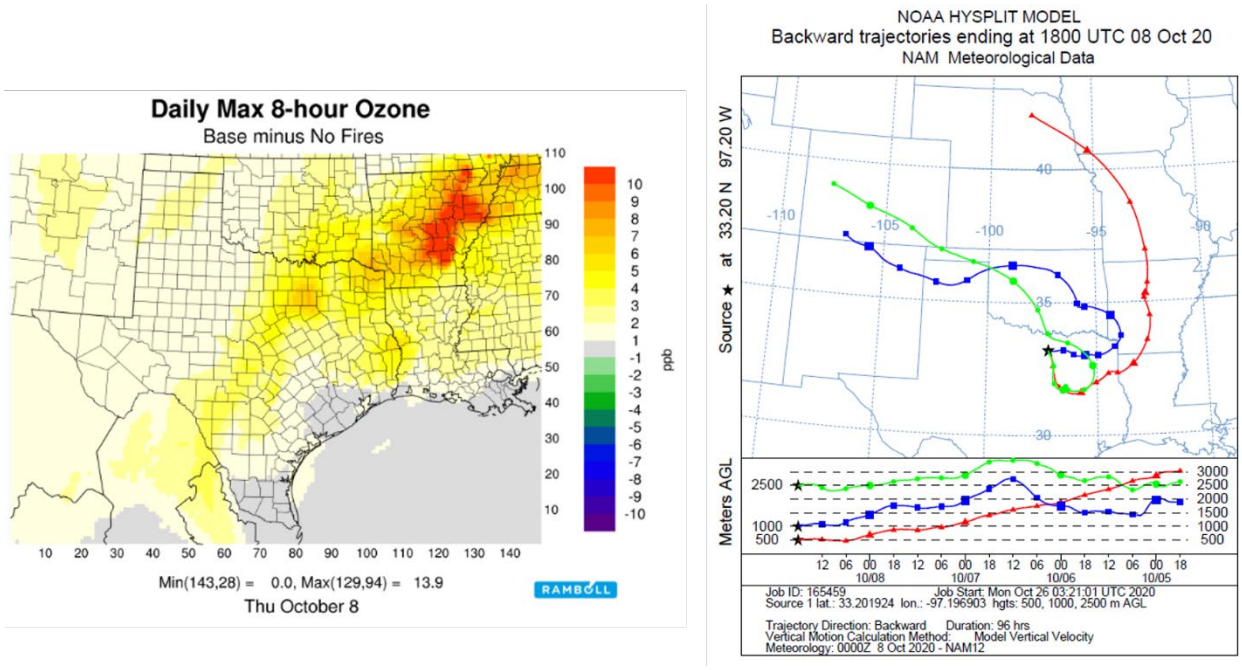


**Figure 5-5. Left panel: NRTEEM fire impacts on MDA8 ozone within the 12 km grid. Right panel: HYSPLIT back trajectories ending at CAMS 56 at the time of peak 1-hour ozone. Back trajectories ending at 500 m (red), 1,000 m (blue) and 2,500 m (green) above CAMS 56 are shown.**

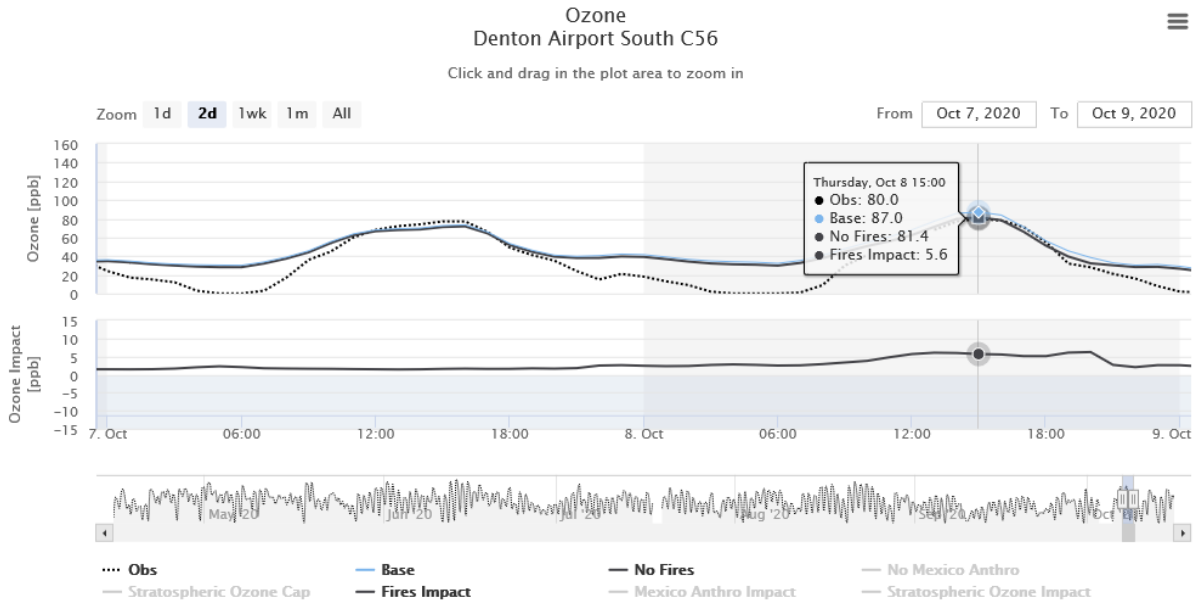


**Figure 5-6. Observed (black dotted line), base model (blue) and No Fires sensitivity run differences from base model (black) ozone time series for October 7-8, 2020 at the Denton Airport South CAMS 56 monitoring site.**

On October 7, wildfire activity in the Mississippi Valley intensified. In

, wildfires are visible along the Mississippi Valley into East Texas. Smoke from Wyoming fires is visible in the DFW area and over the Texas Panhandle. Clouds from Hurricane Delta prevented retrieval of thermal anomalies from fires and AOD over East Texas. On October 7, NRTEEM shows smoke and ozone impacts from a large number of small fires in the Mississippi Valley and East Texas (Figure 5-8). Between October 7 and October 8, the NRTEEM $PM_{2.5}$ and fire ozone impact animations show southeasterly winds over East Texas bringing the fire-affected air toward the DFW area. By October 8 (Figure 5-9), there is a large, diffuse area of enhanced $PM_{2.5}$ and ozone impacts from the fires over the DFW area, other parts of North Texas, Oklahoma and Arkansas. By 3 PM, Hurricane Delta was moving inland and an area of clear air was present along the Texas coastline.

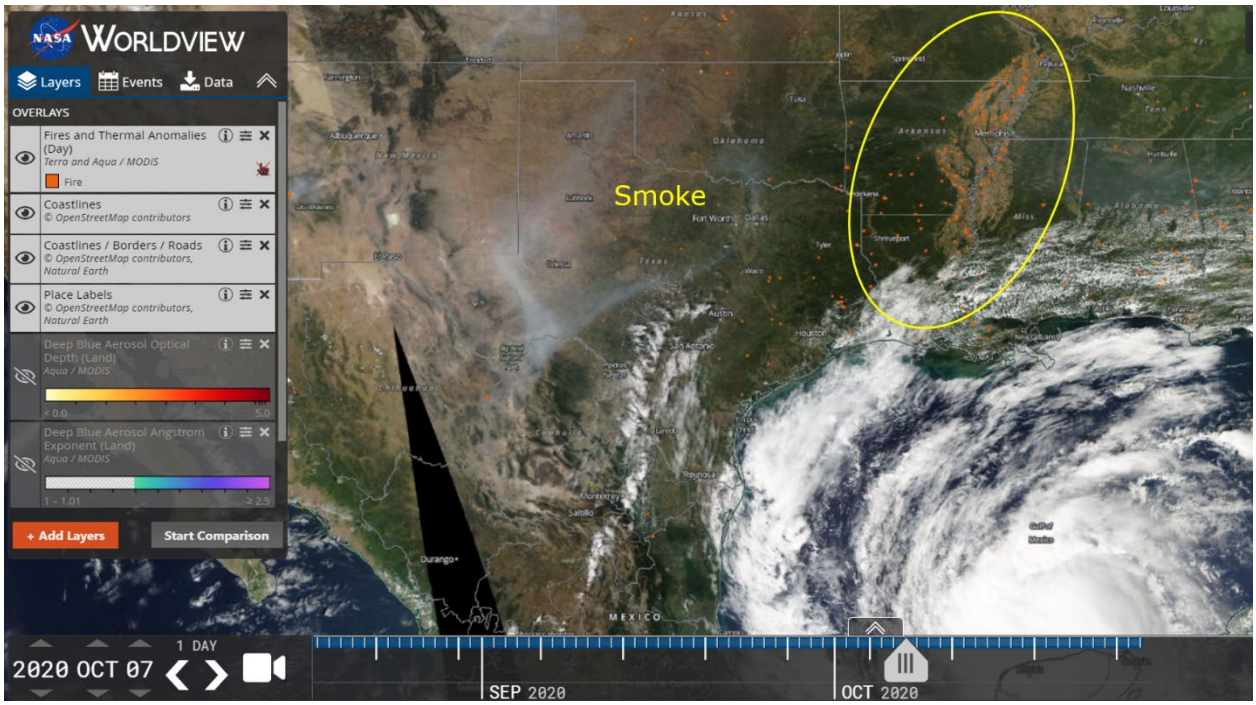


**Figure 5-7. NASA EOSDIS Worldview plots of wildfires (orange icons) along the Mississippi Valley (yellow oval). Smoke transported south from the Wyoming/Colorado wildfires is visible over the Texas Panhandle and the DFW area. Hurricane Delta is visible in the Gulf of Mexico and southeast Texas.**

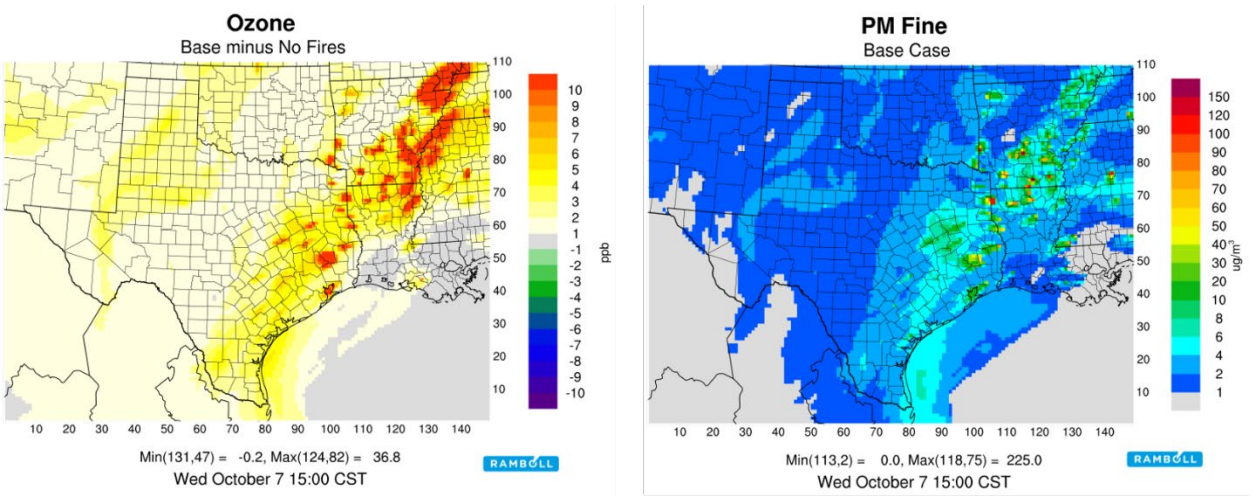


**Figure 5-8. Left panel: NRTEEM fire impacts on MDA8 ozone within the 12 km grid at 3 PM CST on October 7. Right panel: NRTEEM 1-hour average $PM_{2.5}$ within the 36 km grid at 3 PM CST on October 7.**

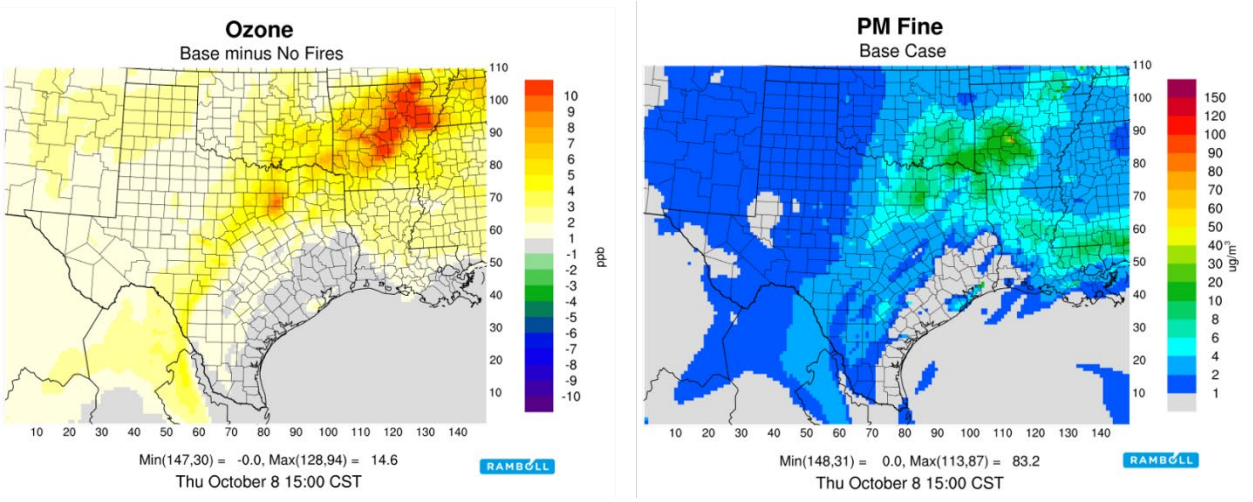


**Figure 5-9. Left panel: NRTEEM fire impacts on MDA8 ozone within the 12 km grid at 3 PM CST on October 8. Right panel: NRTEEM 1-hour average $PM_{2.5}$ within the 36 km grid at 3 PM CST on October 8.**

Much of the smoke transported into Texas on October 8 resulted from fires in the Mississippi Valley on October 7. Therefore, we focus our analysis of this event on October 7.

#### 5.2.3.1 Graphical Comparison of $PM_{2.5}$ Fire Emissions

Figure 5-10 shows the same satellite fire detections (red triangles) and NOAA HMS diagnosed smoke as in Figure 5-3 but for October 7, 2020. The approximate extent for our FEI comparison is shown in blue. Figure 5-11 presents spatial maps of daily total $PM_{2.5}$ emissions on October 7, 2020 for FINN1.0 (left), GFAS1.2 (middle) and QFED2.5 (right). The spatial pattern of emissions for FINN2.5 are similar to QFED2.5. The GFAS1.2 plot shows substantially less fires than the other two plots. Focusing on the Mississippi River Valley, the FINN2.5 plot shows a tighter range in magnitude (mostly below 10 tpd) compared to the QFED2.5 plot (less than 1 to over 100 tpd). The

FINN2.5 plot also shows emissions near Houston, which do not appear on either the QFED2.5 or GFAS1.2 plots. These are likely gas flares mischaracterized as fires, a common issue with FINN1.0 that we have observed with the NRTEEM system (Johnson et al., 2019) and other modeling efforts.

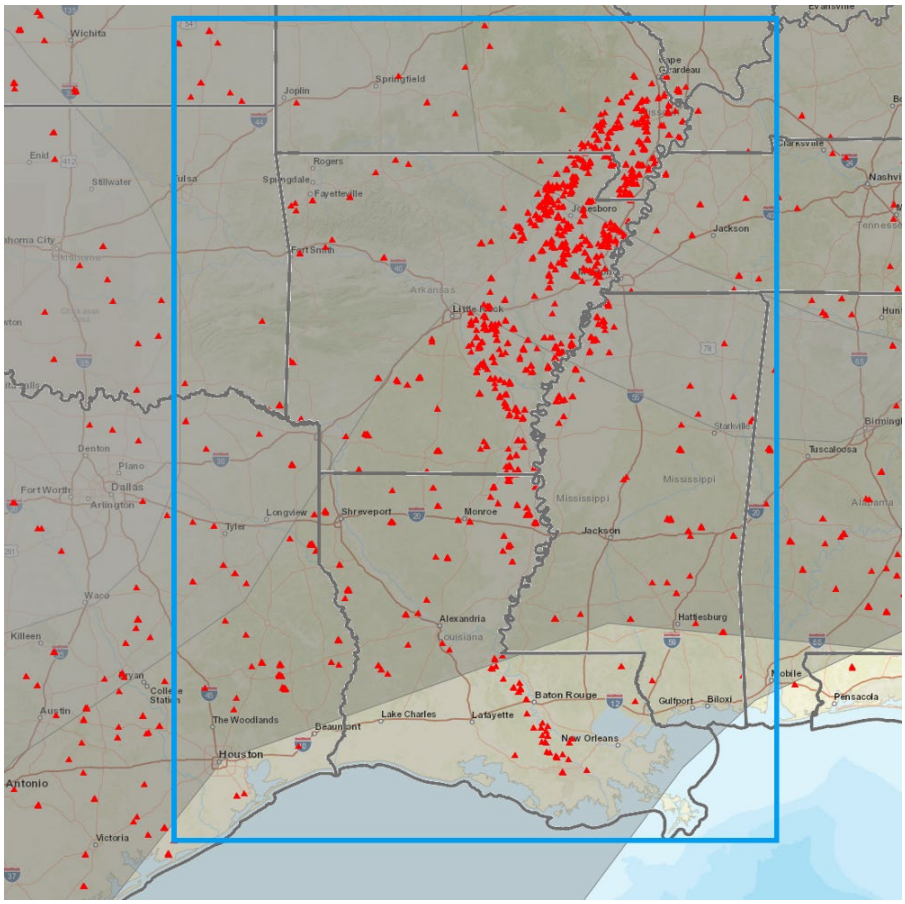


**Figure 5-10. NOAA satellite fire detections (red triangles) and diagnosed smoke on October 7, 2020 (image developed using online tools at Airnowtech.org). The approximate spatial extent for the FEI comparison in Figure 5-11 is shown in blue.**

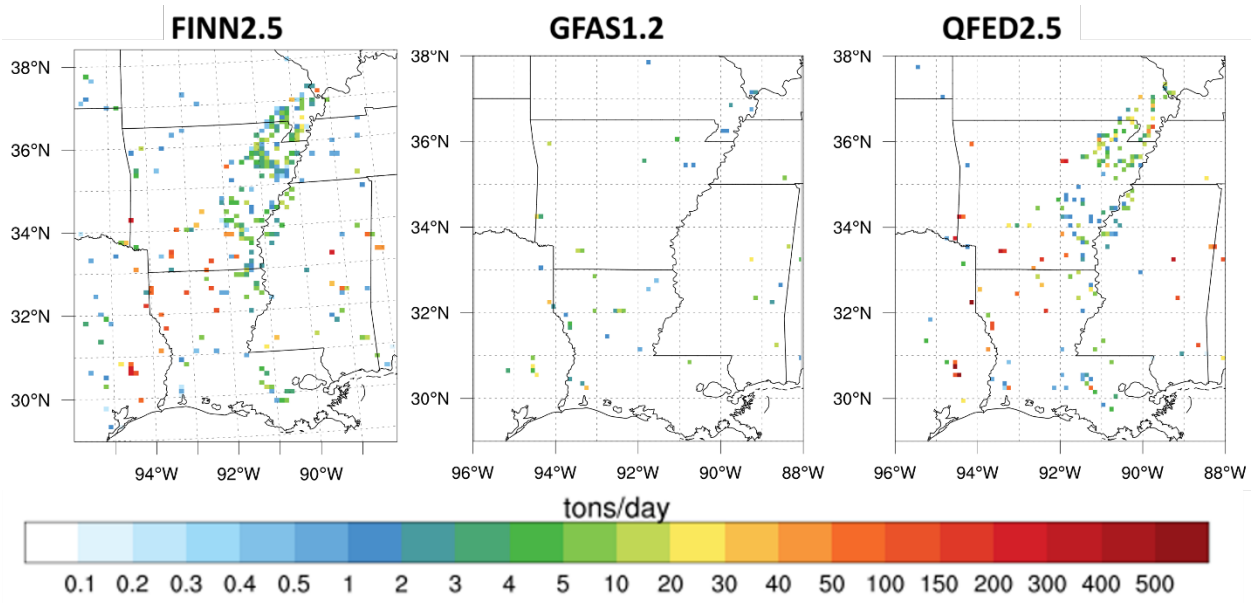


**Figure 5-11. Daily total $PM_{2.5}$ fire emissions for FINN2.5 (left), GFAS1.2 (middle) and QFED2.5 (right) on October 7, 2020.**

#### 5.2.3.2 Emissions Summaries

Table 5-5 presents daily total NOx, VOC, $PM_{2.5}$ and CO emissions for FINN2.5, GFAS1.2 and QFED2.5 over the area shown in Figure 5-11. GFAS1.2 emissions are very small for all species compared to both QFED2.5 and FINN2.5, which agrees with the spatial comparison in Figure 5-11. While FINN2.5 VOC emissions are substantially larger than QFED2.5 (29x), FINN2.5 $PM_{2.5}$ emissions are less than QFED2.5 $PM_{2.5}$ emissions (FINN2.5: 4,578 tpd; QFED2.5: 6,603 tpd).

**Table 5-5. Emissions summaries for FINN1.0, GFAS1.2 and QFED2.5 on October 7, 2020. Spatial extent of area comparison is as shown in Figure 5-10.**

| | Emissions (tons/day) | | |
|---|---|---|---|
| **Species** | **FINN2.5** | **GFAS1.2** | **QFED2.5** |
| NOx | 1,359 | 65 | 855 |
| VOC | 24,679 | 183 | 842 |
| $PM_{2.5}$ | 4,578 | 319 | 6,603 |
| CO | 43,027 | 2,989 | 18,316 |

# 6.0 CONCLUSIONS AND RECOMMENDATIONS

Ramboll developed a new literature-based Python FEI processor that provides the TCEQ a flexible fire emissions processing platform that can process four different FEIs which are 1) FINN1.0; 2) FINN2.5; 3) GFAS1.2 and 4) QFED2.5. The design of the FEI processor allows efficient future customization.

Comparisons of the three FEIs (we chose to evaluate FINN2.5 over FINN1.0 because it is the latest version available and is more similar to the FINN2.2 product that TCEQ is familiar with) revealed substantial differences in emissions of key pollutants for the 2019 ozone season in Texas as well as states that frequently contribute wildfire smoke into Texas. This finding is consistent with the literature review and highlights the uncertainties in fire detection and emissions estimations derived from satellite measurements. Testing and evaluation in CAMx can help to refine the emissions estimates produced by the FEI processor.

Ramboll proposes four activities to improve the FEI processor and support TCEQ's needs:

- Code modifications to process one additional FEI – NASA's FEER1.0-G1.2 product – that could provide better fire emissions estimates for those fires that contribute wildfire smoke into Texas.
- Implement alternative schemes for vertical plume rise (the Sofiev scheme) and temporal allocation (after literature review).
- Recommend potential strategies for combining the available FEI estimates into a consensus FEI.
- Conduct CAMx simulations for one or two 2019 ozone episodes using the five FEIs and evaluate ozone and $PM_{2.5}$ model performance against observations.

# 7.0 REFERENCES

Air Sciences, Inc. 2004. 2002 Fire Emission Inventory for the WRAP Region Phase I – Essential Documentation, Draft Rep. Air Sciences, Inc., Denver, CO.

Akagi, S. K., Yokelson, R. J., Wiedinmyer, C., Alvarado, M. J., Reid, J. S., Karl, T., Crounse, J. D., and Wennberg, P. O. 2011. Emission factors for open and domestic biomass burning for use in atmospheric models, Atmos. Chem. Phys., 11, 4039–4072, https://doi.org/10.5194/acp-11-4039-2011.

Andreae, M. O. and Merlet, P. 2001. Emission of trace gases and aerosols from biomass burning, Global Biogeochem. Cy., 15, 955–966, https://doi.org/10.1029/2000GB001382.

Briggs, G. 1969. Plume rise. Tech. Rep. Crit. Rev. Ser. (p. 81). Springfield, VA: National Technical Information Service.

Darmenov, A. and da Silva, A. 2015. The quick fire emissions dataset (QFED) – Documentation of versions 2.1, 2.2 and 2.4. NASA//TM-2015-104606, Vol. 38, NASA Global Modeling and Assimilation Office, 183 pp., https://gmao.gsfc.nasa.gov/pubs/docs/Darmenov796.pdf

Freeborn, P. H., M. J. Wooster, D. P. Roy, and M. A. Cochrane. 2014. Quantification of MODIS fire radiative power (FRP) measurement uncertainty for use in satellite-based active fire characterization and biomass burning estimation, Geophys. Res. Lett.,41,1988–1994, doi:10.1002/2013GL059086.

Giglio, L., J. Descloitres, C. O. Justice, and Y. Kaufman. 2003. An enhanced contextual fire detection algorithm for MODIS, Remote Sens.Environ.,87, 273–282.

Giglio, L., Randerson, J. T., van der Werf, G. R., Kasibhatla, P. S., Collatz, G. J., Morton, D. C., and DeFries, R. S. 2010. Assessing variability and long-term trends in burned area by merging multiple satellite fire products, Biogeosciences, 7, 1171–1186, https://doi.org/10.5194/bg-7-1171-2010.

Giglio, L. 2013. MODIS Collection 5 Active Fire Product User's Guide, Version 2.5, 61 pp., Dep. of Geogr., Univ. of Maryland, College Park, Md.

Giglio, L., J. Descloitres, C. O. Justice, and Y. Kaufman (2003), An enhanced contextual fire detection algorithm for MODIS, Remote Sens.Environ.,87, 273–282.

Ichoku, C. and Ellison, L. 2014. Global top-down smoke-aerosol emissions estimation using satellite fire radiative power measurements, Atmos. Chem. Phys., 14, 6643–6667, https://doi.org/10.5194/acp-14-6643-2014.

Ichoku, C. and Kaufman, Y. 2005. A Method to Derive Smoke Emission Rates From MODIS Fire Radiative Energy Measurements. Geoscience and Remote Sensing, IEEE Transactions on. 43. 2636 - 2649. 10.1109/TGRS.2005.857328. doi:10.1109/TGRS.2005.857328

Johnson, J., G. Wilson, D.J. Rasmussen, G. Yarwood. 2016. "Daily Near Real-Time Ozone Modeling for Texas." Prepared for Texas Commission on Environmental Quality, Austin, TX. January.

Johnson, J., G. Wilson, M. Jimenez, T. Shah, R. Beardsley and G. Yarwood. 2017. "Fire Impact Modeling with CAMx." Prepared for Texas Commission on Environmental Quality (TCEQ), TX. July.

Johnson, J., G. Wilson, J. Bandoro, K. Richman, L. Huang, R. Beardsley and G. Yarwood, 2018. Near-Real Time Exceptional Event Modeling. Prepared for Mark Estes, TCEQ. August 2018.

Johnson, J., G. Wilson, S. Kemball-Cook, K. Tanner, Y. Shi, J. Guo, R. Beardsley and G. Yarwood. 2019. Near Real-Time Exceptional Event Modeling. Prepared for Mark Estes, TCEQ. August.

Kaiser, J. W., Heil, A., Andreae, M. O., Benedetti, A., Chubarova, N., Jones, L., Morcrette, J.-J., Razinger, M., Schultz, M. G., Suttie, M., and van der Werf, G. R. 2012. Biomass burning emissions estimated with a global fire assimilation system based on observed fire radiative power, Biogeosciences, 9, 527–554, https://doi.org/10.5194/bg-9-527-2012.

Kaufman, Y. J., C. O. Justice, L. P. Flynn, J. D. Kendall, E. M. Prins, L. Giglio, D. E. Ward, W. P. Menzel, and A. W. Setzer (1998), Potential global fire monitoring from EOS-MODIS, J. Geophys. Res.,103(D24), 32,215–32,338.

Larkin, N. K., S. M. O'Neill, R. Solomon, S. Raffuse, T. Strand, D. C. Sullivan, C. Krull, M. Rorig, J. Peterson, and S. A. Ferguson. 2009. The BlueSky smoke modeling framework. Int. J. Wildland Fire 18 (8):906-920. doi: 10.1071/WF07086.

Larkin, N.K.; Raffuse, S. 2015. 2014 Fire NEI workshop: Emissions Processing – SmartFire Details. https://www.epa.gov/sites/default/files/2015-09/documents/emissions_processing_sf2.pdf.

Li, Y., Tong, D.Q., Ngan, F., Cohen, M.D., Stein, A.F., Kondragunta, S., Zhang, X., Ichoku, C., Hyer, E.J. and Kahn, R.A., 2020. Ensemble PM2.5 forecasting during the 2018 Camp Fire event using the HYSPLIT transport and dispersion model. Journal of Geophysical Research: Atmospheres, 125(15), e2020JD032768 (DOI: 10.1029/2020JD032768).

McDonald-Buller, E., Y. Kimura, C. Wiedinmyer, C. Emery, Z. Liu and G. Yarwood. 2015. Targeted Improvements in the Fire INventory from NCAR (FINN) Model for Texas Air Quality Planning. Prepared for David Sullivan, Texas Air Quality Research Program and The University of Texas at Austin. August.

Pan, X., Ichoku, C., Chin, M., Bian, H., Darmenov, A., Colarco, P., Ellison, L., Kucsera, T., da Silva, A., Wang, J., Oda, T., and Cui, G.: Six global biomass burning emission datasets: intercomparison and application in one global aerosol model, Atmos. Chem. Phys., 20, 969–994, https://doi.org/10.5194/acp-20-969-2020, 2020.

Ramboll, 2020. Near Real-Time Exceptional Event Modeling. Prepared for Erik Gribbin, TCEQ. November.

Ramboll Environ, 2016. Review of Fire Plume Rise Algorithms and Recommendations for SMOKE/CMAQ, Ramboll Environ US Corporation, Technical Memorandum prepared for Alison Eyth, US EPA/OAQPS.

Randles, C. A., da Silva, A. M., Buchard, V., Colarco, P. R., Darmenov, A., Govindaraju, R., Smirnov, A., Holben, B., Ferrare, R., Hair, J., Dhinozuka, Y., and Flynn, C. J. 2017. The MERRA-2 aerosol reanalysis, 1980 onward. Part I: system description and data assimilation evaluation, J. Climate, 30, 6823–6850, https://doi.org/10.1175/JCLI-D-16-0609.1.

Reid, J. S., Hyer, E. J., Prins, E. M., Westphal, D. L., Zhang, J., Wang, J., Chistopher, S. A., Curtis, C. A., Schmidt, C. C., Eleuterio, D. P., Richardson, K. A., and Hoffman. J. P. 2009. Global monitoring and forecasting of biomass-burning smoke: Description of and lessons from the Fire Locating and Modeling of Burning Emissions (FLAMBE) program. IEEE Journal of Selected Topics in Applied Earth Observations and Remote Sensing,2(3), 144–162.

Reid, J. S., Koppmann, R., Eck, T. F., and Eleuterio, D. P. 2005. A review of biomass burning emissions part II: intensive physical properties of biomass burning particles, Atmos. Chem. Phys., 5, 799–825, https://doi.org/10.5194/acp-5-799-2005.

Rémy, S., Veira, A., Paugam, R., Sofiev, M., Kaiser, J. W., Marenco, F., Burton, S. P., Benedetti, A., Engelen, R. J., Ferrare, R., and Hair, J. W. 2017. Two global data sets of daily fire emission injection heights since 2003, Atmos. Chem. Phys., 17, 2921–2942, https://doi.org/10.5194/acp-17-2921-2017.

Rienecker, M. M., Suarez, M. J., Gelaro, R., Todling, R., Bacmeister, J., Liu, E., Bosilovich, M. G., Schubert, S. D., Takacs, L., Kim, G.-K., Bloom, S., Chen, J., Collins, D., Conaty, A., da Silva, A., Gu, W., Joiner, J., Koster, R. D., Lucchesi, R., Molod, A., Owens, T., Pawson, S., Pegion, P., Redder, C. R., Reichle, R., Robertson, F. R., Ruddick, A. G., Sienkiewicz, M., and Woollen, J. 2011. MERRA – NASA's Modern-Era Retrospective Analysis for Research and Applications, J. Climate, 24, 3624–3648.

Rolph, G., Stein, A., and Stunder, B. 2017. Real-time Environmental Applications and Display sYstem: READY. Environmental Modelling & Software, 95, 210-228, https://doi.org/10.1016/j.envsoft.2017.06.025.

Sofiev, M., Vankevich, R., Lotjonen, M., Prank, M., Petukhov, V., Ermakova, T., Koskinen, J., and Kukkonen, J. 2009. An operational system for the assimilation of the satellite information on wildland fires for the needs of air quality modelling and forecasting, Atmos. Chem. Phys., 9, 6833–6847, doi:10.5194/acp-9-6833-2009

Sofiev, M., Ermakova, T., & Vankevich, R. 2012. Evaluation of the smoke-injection height from wild-land fires using remote-sensing data. Atmospheric Chemistry and Physics, 12(4), 1995–2006. https://doi.org/10.5194/acp-12-1995-2012

van der Werf, G. R., Randerson, J. T., Giglio, L., Collatz, G. J., Mu, M., Kasibhatla, P. S., Morton, D. C., DeFries, R. S., Jin, Y., and van Leeuwen, T. T. 2010. Global fire emissions and the contribution of deforestation, savanna, forest, agricultural, and peat fires (1997–2009), Atmos. Chem. Phys., 10, 11707–11735, https://doi.org/10.5194/acp-10-11707-2010.

van der Werf, G. R., Randerson, J. T., Giglio, L., van Leeuwen, T. T., Chen, Y., Rogers, B. M., Mu, M., van Marle, M. J. E., Morton, D. C., Collatz, G. J., Yokelson, R. J., and Kasibhatla, P. S. 2017. Global fire emissions estimates during 1997–2016, Earth Syst. Sci. Data, 9, 697–720, https://doi.org/10.5194/essd-9-697-2017.

van Leeuwen, T. T., van der Werf, G. R., Hoffmann, A. A., Detmers, R. G., Rücker, G., French, N. H. F., Archibald, S., Carvalho Jr., J. A., Cook, G. D., de Groot, W. J., Hély, C., Kasischke, E. S., Kloster, S., McCarty, J. L., Pettinari, M. L., Savadogo, P., Alvarado, E. C., Boschetti, L., Manuri, S., Meyer, C. P., Siegert, F., Trollope, L. A., and Trollope, W. S. W. 2014. Biomass burning fuel consumption rates: a field measurement database, Biogeosciences, 11, 7305–7329, https://doi.org/10.5194/bg-11-7305-2014.

van Marle, M. J. E., Kloster, S., Magi, B. I., Marlon, J. R., Daniau, A.-L., Field, R. D., Arneth, A., Forrest, M., Hantson, S., Kehrwald, N. M., Knorr, W., Lasslop, G., Li, F., Mangeon, S., Yue, C., Kaiser, J. W., and van der Werf, G. R. 2017. Historic global biomass burning emissions for CMIP6 (BB4CMIP) based on merging satellite observations with proxies and fire models (1750–2015), Geosci. Model Dev., 10, 3329–3357, https://doi.org/10.5194/gmd-10-3329-2017.

Wiedinmyer, C., Akagi, S.K., Yokelson, R.J., Emmons, L.K., Al-Saadi, J.A., Orlando, J.J. and Soja, A.J., 2011. The Fire INventory from NCAR (FINN): A high resolution global model to estimate the emissions from open burning. Geoscientific Model Development, 4(3), pp.625-641 (DOI: 10.5194/gmd-4-625-2011).

Wiedinmyer, C., Kimura, Y., McDonald-Buller, E., Seto, K., Emmons, L., Tang, W., Buchholz, R., Orlando, J. The Fire INventory from NCAR version 2 (FINNv2): updates to a high resolution global fire emissions model. In preparation for submission to the Journal of Advances in Modeling Earth Systems.

Wilkins, J. L., Pouliot, G., Pierce, T., Soja, A., Choi, H., Gargulinski, E., Gilliam, R., Vukovich, J., Landis, M. S. 2022. An evaluation of empirical and statistically based smoke plume injection height parametrisations used within air quality models. International Journal of Wildland Fire 31, 193-211. https://doi.org/10.1071/WF20140

Zhang, X., Kondragunta, S., Da Silva, A., Lu, S., Ding, H., Li, F., & Zhu, Y. (2019). The blended global biomass burning emissions product from MODIS and VIIRS observations (GBBEPx) version 3.1, https://www.ospo.noaa.gov/Products/land/gbbepx/docs/GBBEPx_ATBD.pdf

# APPENDIX A

## Detailed Emission Summaries

# Appendix A Detailed Emission Summaries

This appendix includes the same emissions summaries as in Table 5-1 and Table 5-2, but includes all U.S. states, in addition to Canada and Mexico.

**Table A-1. $PM_{2.5}$ and NOx emissions summaries for FINN2.5, GFAS1.2 and QFED2.5 for April 1 – October 31, 2019.**

| State | $PM_{2.5}$ (tons) | | | NOx (tons) | | |
|---|---|---|---|---|---|---|
| | FINN2.5 | GFAS1.2 | QFED2.5 | FINN2.5 | GFAS1.2 | QFED2.5 |
| Alabama | 50,814 | 8,673 | 92,818 | 11,743 | 1,696 | 6,871 |
| Arkansas | 29,441 | 4,674 | 45,369 | 8,774 | 755 | 8,290 |
| Arizona | 16,912 | 23,775 | 131,006 | 6,875 | 6,173 | 17,225 |
| California | 55,106 | 40,724 | 180,636 | 14,406 | 10,106 | 23,871 |
| Colorado | 2,083 | 6,477 | 26,374 | 1,106 | 1,847 | 6,284 |
| Connecticut | 195 | 44 | 777 | 46 | 7 | 62 |
| D.C. | 0 | 1 | 1 | 0 | 0 | 1 |
| Delaware | 180 | 154 | 247 | 78 | 46 | 70 |
| Florida | 33,772 | 14,102 | 67,676 | 11,218 | 3,038 | 14,643 |
| Georgia | 42,565 | 10,028 | 70,606 | 11,320 | 1,974 | 7,995 |
| Iowa | 3,514 | 1,297 | 9,639 | 1,934 | 173 | 4,325 |
| Idaho | 45,852 | 16,902 | 126,130 | 9,538 | 3,963 | 11,759 |
| Illinois | 2,853 | 779 | 6,003 | 1,149 | 99 | 1,425 |
| Indiana | 2,079 | 340 | 2,205 | 740 | 48 | 622 |
| Kansas | 9,594 | 14,765 | 52,629 | 6,060 | 4,286 | 21,948 |
| Kentucky | 5,773 | 437 | 4,277 | 1,625 | 76 | 858 |
| Louisiana | 36,631 | 7,492 | 70,342 | 9,129 | 1,459 | 7,504 |
| Massachusetts | 363 | 298 | 2,175 | 89 | 63 | 301 |
| Maryland | 819 | 368 | 1,486 | 248 | 105 | 296 |
| Maine | 412 | 121 | 554 | 90 | 23 | 44 |
| Michigan | 4,277 | 2,567 | 9,361 | 1,033 | 502 | 997 |
| Minnesota | 6,710 | 2,559 | 15,464 | 2,915 | 467 | 5,743 |
| Missouri | 9,042 | 1,802 | 15,527 | 3,634 | 294 | 4,092 |
| Mississippi | 27,626 | 3,049 | 31,412 | 7,071 | 434 | 4,181 |
| Montana | 16,756 | 9,181 | 62,653 | 4,170 | 2,068 | 7,698 |
| North Carolina | 16,934 | 8,445 | 39,589 | 4,725 | 1,573 | 4,341 |
| North Dakota | 8,286 | 2,128 | 13,775 | 4,794 | 335 | 6,168 |
| Nebraska | 1,575 | 846 | 4,228 | 898 | 154 | 1,890 |
| New Hampshire | 121 | 175 | 1,190 | 37 | 35 | 73 |
| New Jersey | 374 | 209 | 1,200 | 136 | 32 | 210 |
| New Mexico | 2,224 | 6,351 | 40,551 | 1,249 | 1,549 | 5,945 |
| Nevada | 560 | 2,081 | 8,199 | 308 | 641 | 3,254 |
| New York | 843 | 151 | 2,287 | 277 | 31 | 169 |
| Ohio | 1,618 | 391 | 2,855 | 494 | 58 | 816 |

| State | $PM_{2.5}$ (tons) | | | NOx (tons) | | |
|---|---|---|---|---|---|---|
| | FINN2.5 | GFAS1.2 | QFED2.5 | FINN2.5 | GFAS1.2 | QFED2.5 |
| Oklahoma | 12,896 | 7,421 | 35,290 | 5,562 | 1,990 | 10,287 |
| Oregon | 77,744 | 13,267 | 112,418 | 15,186 | 2,874 | 9,645 |
| Pennsylvania | 3,057 | 748 | 8,602 | 872 | 78 | 1,083 |
| Rhode Island | 46 | 71 | 802 | 10 | 13 | 100 |
| South Carolina | 11,870 | 3,865 | 20,981 | 2,989 | 710 | 2,442 |
| South Dakota | 560 | 190 | 1,120 | 316 | 28 | 472 |
| Tennessee | 7,576 | 760 | 7,119 | 2,290 | 79 | 1,191 |
| Texas | 33,311 | 14,820 | 95,027 | 11,487 | 3,559 | 18,040 |
| Utah | 1,459 | 4,662 | 20,717 | 965 | 1,210 | 4,499 |
| Virginia | 13,162 | 2,859 | 36,570 | 2,996 | 511 | 2,386 |
| Vermont | 290 | 10 | 78 | 58 | 2 | 5 |
| Washington | 42,302 | 13,947 | 86,569 | 9,054 | 3,044 | 10,884 |
| Wisconsin | 3,569 | 1,394 | 6,321 | 1,205 | 266 | 1,343 |
| West Virginia | 10,550 | 357 | 5,907 | 2,017 | 41 | 365 |
| Wyoming | 1,304 | 3,337 | 14,701 | 756 | 796 | 2,458 |
| Contiguous U.S. | 655,600 | 259,093 | 1,591,464 | 183,675 | 59,309 | 245,173 |
| Canada | 1,314,301 | 1,371,052 | 1,820,826 | 173,920 | 269,099 | 126,954 |
| Mexico | 2,041,475 | 447,427 | 1,868,173 | 719,702 | 90,844 | 289,160 |

**Table A-2. VOC and CO emissions summaries for FINN2.5, GFAS1.2 and QFED2.5 for April 1 – October 31, 2019.**

| State | VOC (tons) | | | CO (tons) | | |
|---|---|---|---|---|---|---|
| | FINN2.5 | GFAS1.2 | QFED2.5 | FINN2.5 | GFAS1.2 | QFED2.5 |
| Alabama | 219,510 | 6,125 | 14,022 | 422,435 | 85,848 | 188,174 |
| Arkansas | 163,814 | 3,514 | 10,006 | 276,381 | 51,000 | 152,635 |
| Arizona | 68,434 | 25,991 | 24,602 | 139,568 | 254,043 | 358,189 |
| California | 221,797 | 45,544 | 33,999 | 411,136 | 424,232 | 495,357 |
| Colorado | 9,564 | 7,767 | 6,753 | 18,566 | 75,243 | 106,757 |
| Connecticut | 850 | 13 | 120 | 1,639 | 545 | 1,633 |
| D.C. | 0 | 0 | 0 | 1 | 6 | 8 |
| Delaware | 1,045 | 200 | 70 | 1,769 | 1,987 | 1,136 |
| Florida | 146,281 | 12,044 | 16,381 | 285,899 | 147,625 | 255,698 |
| Georgia | 184,561 | 6,662 | 12,436 | 358,571 | 100,815 | 177,191 |
| Iowa | 35,383 | 1,319 | 3,764 | 47,843 | 16,107 | 63,960 |
| Idaho | 164,661 | 16,273 | 20,602 | 314,662 | 169,839 | 285,501 |
| Illinois | 19,875 | 328 | 1,534 | 30,527 | 8,870 | 24,233 |
| Indiana | 12,701 | 233 | 626 | 20,579 | 5,177 | 10,114 |
| Kansas | 58,161 | 14,725 | 19,488 | 96,901 | 185,386 | 328,749 |
| Kentucky | 28,128 | 239 | 992 | 50,483 | 5,525 | 15,333 |

| State | VOC (tons) | | | CO (tons) | | |
|---|---|---|---|---|---|---|
| | FINN2.5 | GFAS1.2 | QFED2.5 | FINN2.5 | GFAS1.2 | QFED2.5 |
| Louisiana | 173,255 | 5,249 | 12,095 | 315,359 | 73,877 | 170,861 |
| Massachusetts | 1,578 | 108 | 418 | 3,084 | 3,244 | 6,137 |
| Maryland | 3,968 | 437 | 343 | 7,269 | 4,632 | 5,298 |
| Maine | 1,815 | 72 | 85 | 3,433 | 1,084 | 1,158 |
| Michigan | 19,023 | 2,081 | 1,609 | 35,366 | 22,432 | 22,724 |
| Minnesota | 52,314 | 2,846 | 5,275 | 77,183 | 29,317 | 87,920 |
| Missouri | 55,588 | 1,373 | 4,226 | 90,395 | 21,553 | 67,674 |
| Mississippi | 131,106 | 1,429 | 5,931 | 240,937 | 30,145 | 86,509 |
| Montana | 63,955 | 8,084 | 11,421 | 123,246 | 88,472 | 164,661 |
| North Carolina | 75,219 | 5,956 | 6,882 | 144,531 | 75,070 | 97,608 |
| North Dakota | 75,643 | 2,700 | 5,372 | 106,020 | 25,631 | 91,262 |
| Nebraska | 14,947 | 803 | 1,647 | 20,655 | 10,721 | 27,974 |
| New Hampshire | 526 | 59 | 170 | 1,034 | 1,502 | 2,222 |
| New Jersey | 1,758 | 69 | 259 | 3,373 | 2,223 | 3,927 |
| New Mexico | 9,832 | 6,322 | 8,008 | 19,594 | 65,283 | 118,421 |
| Nevada | 2,536 | 2,680 | 2,930 | 4,761 | 25,705 | 49,178 |
| New York | 4,089 | 84 | 345 | 7,593 | 1,972 | 4,636 |
| Ohio | 8,712 | 97 | 818 | 14,955 | 5,618 | 13,230 |
| Oklahoma | 62,028 | 6,743 | 10,237 | 113,186 | 91,609 | 165,953 |
| Oregon | 271,103 | 11,350 | 17,828 | 525,544 | 125,029 | 244,181 |
| Pennsylvania | 14,378 | 145 | 1,585 | 26,427 | 7,907 | 22,931 |
| Rhode Island | 201 | 8 | 147 | 383 | 884 | 2,124 |
| South Carolina | 50,747 | 2,038 | 3,738 | 98,841 | 35,394 | 53,474 |
| South Dakota | 5,505 | 164 | 418 | 7,511 | 2,382 | 7,062 |
| Tennessee | 36,017 | 208 | 1,500 | 66,207 | 8,706 | 22,596 |
| Texas | 148,615 | 11,386 | 21,390 | 282,219 | 170,429 | 328,035 |
| Utah | 7,073 | 4,864 | 5,025 | 13,196 | 50,565 | 78,477 |
| Virginia | 57,444 | 1,665 | 5,319 | 109,817 | 26,106 | 70,190 |
| Vermont | 1,270 | 3 | 11 | 2,381 | 94 | 150 |
| Washington | 157,568 | 13,307 | 15,938 | 297,209 | 131,955 | 230,556 |
| Wisconsin | 19,114 | 1,130 | 1,515 | 33,568 | 14,082 | 23,584 |
| West Virginia | 46,094 | 77 | 846 | 86,031 | 3,158 | 11,093 |
| Wyoming | 6,445 | 3,519 | 3,096 | 12,206 | 33,192 | 46,651 |
| Contiguous U.S. | 2,914,232 | 238,036 | 321,827 | 5,370,473 | 2,722,223 | 4,793,123 |
| Canada | 5,316,001 | 1,419,049 | 270,064 | 8,711,756 | 11,362,217 | 3,595,048 |
| Mexico | 12,075,116 | 530,763 | 441,111 | 18,643,959 | 4,990,173 | 6,493,333 |